Manuscript Details

Manuscript number	PRECAM_2019_203_R1
Title	Episodic magmatism during the growth of a Neoproterozoic oceanic arc (Anti-Atlas, Morocco)
Article type	Research Paper

Abstract

We present an integrated study combining detailed field, geochronological and geochemical data of a Neoproterozoic intra-oceanic arc systems exposed in the Pan-African belt of the Moroccan Anti-Atlas. The arc rock units exposed in Bou Azzer and Sirwa inliers consist of a tectonic patchwork of back-arc ophiolitic sequences to the north thrusted onto accreted arc complexes to the south. Arc complexes are composed of amphibolite, granodioritic and granitic gneisses intruded by various undeformed hydrous ultramafic (hornblendite), mafic (hornblende-gabbro, diorite) and felsic (granodiorite, tonalite, granite) arc lithologies. We show that these complexes are remnants of a long-lived (120 Myr) Neoproterozoic oceanic arc, punctuated by three successive magmatic episodes (760-730 Ma, 710-690 Ma, 660-640 Ma respectively) interspersed with periods of magmatic quiescence. The typical geochemical arc signature and positive ƐNdt values for the igneous rocks emplaced during each magmatic episode (medians at +7.1, +5.4 and +5.7, from older to younger) attest that their parental magmas derived from a depleted mantle source without substantial assimilation by the WAC older crustal basement. Trace-element geochemistry, i.e. Sr/Y, La/Yb, of intermediate to felsic arc rocks produced during each magmatic pulse suggests that the arc crust was thickened (> 30-35 km) over a short time period between the first and second magmatic episodes (730 - 710 Ma) which coincides with an important regional shortening event. Soft-docking of the oceanic arc on a buoyant transitional margin is invoked to explain tectonic inversion in overriding plate, leading to shortening and related thickening of the arc crust. Concomitant magmatic shutdown resulting from a reorganization of subduction dynamics (i.e. change in slab geometry, flip in subduction polarity). A non-tectonic critical thickening of the arc crust is invoked to explain the second magmatic shutdown (680-660 Ma), by freezing the subarc mantle influx. This lull period is followed by a third magmatic episode which is likely triggered by delamination of the dense lower crust and reactivation of subarc mantle flow. This is supported by the bimodal chemical signature of evolved magmatic products, suggesting two distinct sources: partial melts from the foundered lower crust and new magmatic products which differentiated from a post-delamination thinned crust.

Keywords	subduction; oceanic arc; episodic magmatism; Neoproterozoic; arc tempo; arc root delamination

Corresponding Author	Antoine Triantafyllou
Corresponding Author's Institution	Department of Geosciences - University of Arizona
Order of Authors	Antoine Triantafyllou, Julien Berger, Jean-Marc Baele, nadine mattielli, Mihai Ducea, Sarane Sterckx, Scott Samson, Florent HODEL, Nasser Ennih
Suggested reviewers	Susan Debari, Dominique GASQUET, Carlos J. Garrido, Serge lallemand, Scott Paterson

Episodic magmatism during the growth of a Neoproterozoic oceanic arc (Anti-Atlas, Morocco)

Antoine Triantafyllou[1, 2], Julien Berger[3], Jean-Marc Baele[4], Nadine Mattielli[2], M. N. Ducea[1, 5], Sarane Sterckx[6], Scott Samson[7], Florent Hodel[3], Nasser Ennih[8]

[1] Department of Geosciences, University of Arizona, Tucson, Arizona 85721, USA.

[2] Department of Earth and Environmental Sciences – G-Time Laboratory, Université Libre de Bruxelles, 50 Avenue Franklin Roosevelt, 1050 Brussels, Belgium.

[3] Géosciences Environnement Toulouse (GET), Observatoire de Midi-Pyrénées, CNRS, IRD, Université de Paul Sabatier, UMR-CNRS 5563, 14, Avenue Edouard Belin, 31400 Toulouse, France.

[4] Department of Geology and Applied Geology, Université de Mons, 20, Place du Parc, B-7000, Belgium.

[5] Faculty of Geology and Geophysics, University of Bucharest, 010041, Bucharest, Romania.

[6] Goldspot Discoveries Inc., 69 Yonge Street Suite 1010, Toronto, Canada.

[7] Department of Earth Sciences, Syracuse University, Syracuse, NY 13244, USA.

[8] EGGPG, Département de Géologie, Faculté des Sciences, Université Chouaïb Doukkali, 24000 El Jadida, Morocco.

Abstract

We present an integrated study combining detailed field, geochronological and geochemical data of a Neoproterozoic intra-oceanic arc systems exposed in the Pan-African belt of the Moroccan Anti-Atlas. The arc rock units exposed in Bou Azzer and Sirwa inliers consist of a tectonic patchwork of back-arc ophiolitic sequences to the north thrusted onto accreted arc complexes to the south. Arc complexes are composed of amphibolite, granodioritic and granitic gneisses intruded by various undeformed hydrous ultramafic (hornblendite), mafic (hornblende-gabbro, diorite) and felsic (granodiorite, tonalite, granite) arc lithologies. We show that these complexes are remnants of a long-lived (120 Myr) Neoproterozoic oceanic arc, punctuated by three successive magmatic episodes (760-730 Ma, 710-690 Ma, 660-640 Ma respectively) interspersed with periods of magmatic quiescence. The typical geochemical arc signature and positive εNd_t values for the igneous rocks emplaced during each magmatic episode (medians at +7.1, +5.4 and +5.7, from older to younger) attest that their parental magmas derived from a depleted mantle source without substantial assimilation by the WAC older crustal basement. Trace-element geochemistry, *i.e*. Sr/Y, La/Yb, of intermediate to felsic arc rocks produced during each magmatic pulse suggests that the arc crust was thickened (> 30-35 km) over a short time period between the first and second magmatic episodes (730 - 710 Ma) which coincides with an important regional shortening event. Soft-docking of the oceanic arc on a buoyant transitional margin is invoked to explain tectonic inversion in overriding plate, leading to shortening and related thickening of the arc crust. Concomitant magmatic shutdown resulting from a reorganization of subduction dynamics (*i.e.* change in slab geometry, flip in subduction polarity). A non-tectonic critical thickening of the arc crust is invoked to explain the second magmatic shutdown (680-660 Ma), by freezing the subarc mantle influx. This lull period is followed by a third magmatic episode which is likely triggered by delamination of the dense lower crust and reactivation of subarc mantle flow. This is supported by the bimodal chemical signature of evolved magmatic products, suggesting two

distinct sources: partial melts from the foundered lower crust and new magmatic products which differentiated from a post-delamination thinned crust.

Keywords*: subduction; oceanic arc; episodic magmatism; Neoproterozoic; arc tempo; arc root delamination*

1. Introduction

Continental and oceanic arcs are sites of high magmatic productivity which contribute to crustal growth either by direct addition of intermediate magmatic rock into the continental crust at active ocean-continent convergent margins or after tectonic accretion of island arcs formed above ocean-ocean subduction zones (Stern, 2010). Active arcs only provide snapshots of their growth history and they cannot be used to unravel the evolution and building mechanisms of arc systems from a combined petrologic, geochemical, and tectonic perspectives. Instead, fossil arc systems give direct access to deeper sections of the crust and potentially record the long-lived evolution of arc systems. Recent studies on extinct arcs showed that the evolution of arc magmatism may dramatically fluctuate (e.g., Paterson and Ducea, 2015), as in many continental arcs, especially in the west American cordilleras, for which magmatic activity is highly episodic (Armstrong, 1988; Ducea et al., 2015a). Their magmatic evolution is marked by short periods (5–20 Myr) of high magmatic flux, also called flare ups, separated by longer periods (30–40 Myr) of magmatic quiescence (Ducea, 2001; Ducea and Barton, 2007). The origin of this magmatic periodicity is still debated for continental arcs and poorly explored for oceanic arc systems.

Changes in tectonic regime at the subduction zone scale represent an important factor influencing the magmatic activity in arcs. Magmatic flare-ups are thought to operate in conjunction with shortening tectonics in the upper plate during subduction (Ducea and Barton 2007). Analogue and numerical modelling as well as observations of modern subduction systems, especially along the Andean active margin, show that the distribution of magmatic activity, the tectonic regime in the overriding plate and the geometry of the dipping slab can all be highly variable and linked to each other (Gorczyk et al., 2007; Schellart et al., 2007; Heuret et al., 2007; Lallemand et al., 2008; Humphreys, 2009; Guillaume et al., 2009 and references therein). Furthermore, crustal (lithospheric) thickening has also important consequences on the arc magmatic activity and was proposed to be an important precursor of magmatic flare-up in the California arc (Ducea, 2001; DeCelles et al., 2009). Crustal thickening forces filtration

of mantle-derived mafic magmas into the lower crust which in the long term can cause a thermal runaway and subsequent magmatic flare-up (Dufek and Bergantz 2005). At a critical stage, arc crust thickening may even freeze and/or delocalize the mantle wedge convective flux, hence, the activity of the arc magmatic center itself (DeCelles et al., 2009; Ducea et al., 2015b and references therein). Alongside, such crustal thickening also leads the arc root to reach the garnet stability field which induces a local densification of the lower crust. The dense residual lower crust, *i.e*. arclogite, is unstable gravitationally and may eventually founder and/or be convectively removed into the mantle (Currie et al., 2015), which could contribute to the refertilization and the reactivation of the subarc mantle flux (Lee and Anderson, 2015).

Magma productivity in oceanic arcs appears to be more continuous in comparison to continental arc record. Modern oceanic arcs are relatively short lived (maximum of 46 - 75 Ma old for the Aleutian; Jicha and Jagoutz, 2015) and therefore, show limited possibilities for changes in their intra-arc tectonic regimes, magmatism rate and critical thickening of their crust (Lallemand et al., 2005; Gerya, 2011). Nevertheless, numerous studies on accreted oceanic arcs show that, similarly to their continental counterparts, they are subject to crustal thickening, crustal root densification and foundering (Jagoutz and Behn, 2013; Jagoutz and Schmidt, 2013). Nonetheless, compilations of geochronological data made so far on fossil and active arc systems do not reveal a periodicity in their magmatic activity (e.g., Jagoutz et al., 2009; Rioux et al., 2010; Hacker et al., 2011; Jicha and Jagoutz, 2015).

We report in this paper a geochronological and geochemical compilation on the fossil Neoproterozoic oceanic arc system in the Pan-African belt exposed in the Anti-Atlas orogen, Morocco. Although the kinematics and geometry of the subduction system are difficult to constrain, these complexes offer a good record of the former magmatic activity and provide, to the best of our knowledge, the first example of an oceanic arc characterized by episodic magmatism. We discuss the mechanisms which can cause shutdown of magmatism and emphasize the strong interplay between tectonics, magmatism and crustal thickening during the evolution of an oceanic arc. Despite the fact that Neoproterozoic and Phanerozoic belts

exhibit similar features, hence implying comparable plate tectonic processes, we show that differences exist when considering the scale of subduction dynamics.

2. Structure of accreted oceanic units in the Pan-African Anti-Atlas orogen

The Anti-Atlas orogen is the northwesternmost segment of a more than 4000 km-long Pan-African orogenic belt formed after subduction of oceanic and continental slabs as evidenced by the presence of eclogites, blueschists, ophiolitic sequences and accreted arc complexes (Ganade de Araujo et al., 2014; Letsch et al., 2017; Fig. 1a). In the Moroccan Anti-Atlas, fossil oceanic arcs crop out in the southern part of the Sirwa and Bou Azzer windows (Gasquet et al., 2008; Hefferan et al., 2014). They were accreted onto the West African Craton (WAC) margin, consisting of Paleoproterozoic basement and passive margin sedimentary and volcanic sequences (Thomas et al., 2004; Gasquet et al., 2005; Triantafyllou et al., 2016, 2018; Fig. 1b). The ophiolite assemblages exposed in the northern side of both windows have been thrusted to the south onto the fossil arc units (El Hadi et al., 2010; Triantafyllou et al., 2016). They represent the back-arc component of the subduction system (Bodinier et al., 1984; Ahmed et al., 2005; Bousquet et al., 2008; Hodel et al., 2017; 2018) which was dated only in the Sirwa window at 762 Ma (Samson et al., 2004). In both areas, the ophiolite is composed of strongly deformed and metamorphosed serpentinites (former mantle peridotites), layered and isotropic metagabbros and metabasalts. Sm-Nd dating of garnet amphibolites within the Sirwa window constrained amphibolite grade metamorphism at ca. 647 Ma (Inglis et al., 2005; Inglis et al., 2017).

The paleo-arc complexes exposed in the southern side of both inliers consist of a heterogeneous assemblage in terms of lithology, metamorphism and deformation (Blein et al., 2014; Hefferan et al., 2014; Fig. 2). Considering both inliers as a whole, three arc units can be distinguished based on field relations and igneous U-Pb ages:

(i) The gneissic unit forms a discontinuous band of mafic to intermediate and felsic orthogneisses (see orange unit in Fig. 2a-b). In the Sirwa inlier, the Tachakoucht gneisses

represent former andesitic subvolcanic units. In the Bou Azzer window, the gneissic unit is mostly represented by former plutonic rock marking mafic to felsic bimodal magmatism with evidence for magmatic mingling prior to solid state deformation (Fig. 3). Their igneous protoliths were dated between 755 and 730 Ma (Thomas et al., 2002; D'Lemos et al., 2006; Blein et al, 2014; Triantafyllou et al., 2016).

(ii) In the Bou Azzer area, these gneissic rocks are intruded by hydrous ultramafic and mafic arc lithologies (hornblendite and hornblende-gabbro). Their emplacement led to dehydration and dehydration-melting reactions in the garnet stability field and production of intermediate to felsic melts (tonalite, granodiorite and leucogranodiorite; Triantafyllou et al., 2018; Fig. 3a). Emplacement ages for both mafic and felsic igneous rocks are bracketed between 710 and 685 Ma (D'Lemos et al., 2006; El Hadi et al., 2010; Triantafyllou et al., 2018).

(iii) In both inliers, back arc ophiolites and arc units are crosscut by igneous arc rocks. In the Sirwa window, they are represented by hornblende-gabbro and coarse-grained hornblendites intruding the host Tachakoucht gneiss. The thermal pulse induced by the intrusion of these mafic-ultramafic rocks led to localized partial melting of the host gneiss and production of leucogranitic melts (Fig. 3b). The leucogranitic rocks (with large enclaves of hornblendite and hornblende gabbro) were found as intrusive material within the Khzama back arc ophiolite, thus indicating that the latter has been thrusted onto the arc complexes before this last igneous pulse. In the Bou Azzer inlier, quartz-dioritic to granodioritic plutons intrude the back-arc ophiolite as well as the older arc units. U-Pb zircon ages for this unit are clustered between 660 and 640 Ma (Thomas et al., 2002; Triantafyllou et al., 2016; Inglis et al., 2005; El Hadi et al., 2010; Walsh et al., 2012; Fig. 2a).

3. Compilation of previous data and results

Three types of datasets are presented in this paper: *(i)* a compilation of U-Pb ages for arc magmatic rocks published in the literature on the Moroccan arc, *(ii)* bulk rock geochemistry

(major and trace elements) on intermediate to felsic arc-related lithologies and *(iii)* whole-rock Nd isotopic compositions for each igneous arc unit.

3.1 Age distribution of the Moroccan arc magmatic events

We gathered geochronological data published so far on igneous crystalline arc lithologies in the studied area (Fig. 2a). Each U-Pb date is inferred to represent the best estimate of the emplacement of arc magmatic intrusions and/or related high-grade metamorphic events due to the emplacement of an adjacent igneous body (based on zircon rims dates and/or cooling dates when appropriate; see references in appendix C1 for further description; $n = 37$). Compilation of geochronological data evidences along duration of arc magmatism over a period of 100 to 120 Myr (Fig. 4). However, this activity is discontinuous, with a cadence of three successive main events illustrated by peaks of zircon abundance/production interspersed by short periods with minimal to absence of magmatic activity (Fig. 4). These age peaks do not appear to reflect a bias in sampling as a systematic and homogeneous sampling has been conducted on every recognized arc unit in our field study. These peaks are interpreted as successive episodes of arc magma production centered at 753 Ma, 701 Ma and 653 Ma, respectively (median values for each cluster) interspersed by periods of approximately 50 Myr during which magmatic production was either shut down or the rate was substantially lowered. For a broader comparison, the Mesozoic evolution of the Cordilleran continental arc shows a similar episodic behavior with a comparable frequency of 30 to 70 Myr between ages peak interpreted as three successive magmatic flare-ups (Paterson and Ducea, 2015). Quantifying magmatic addition rates requires quantifying apparent volume of magmatic rock emplaced during each magmatic pulse. In this study, we quantified surface area for each igneous group based on detailed geological maps (Admou et al, 2013; Triantafyllou, 2016): 72.4 km² (ca. 52 % of total exposed igneous arc rock in the studied area), 11.2 km² (ca. 8%) and 54.3 km² (ca. 40%) for the first (760-730 Ma), the second (710-690 Ma) and the third (660-640 Ma) magmatic episode respectively. However, it is unlikely that these values reflect the actual magma volume that was originally added to the arc system and thus, cannot be used

188 to give weight to each magmatic pulse and ultimately, to quantify magmatic addition rates
189 during arc life. This is because igneous rocks from fossil oceanic arcs are not emplaced and
190 collected in a stable margin as for continental arc settings but instead, into a non-steady
191 oceanic crust which subsequently endured tectonic accretion and obduction onto a continental
192 margin. Therefore, we do not attempt to quantify volumes of magma produced through each
193 igneous event in this study but we emphasize the pulsed and periodic behavior of the
194 magmatic signal in an intra-oceanic arc setting.
195
196 *3.2 Geochemistry of intermediate to felsic arc rocks*
197 In order to study the evolution of magma composition through time, 51 samples (including 4
198 samples from Bougmane complex; Triantafyllou et al., 2018) were analyzed and grouped
199 according to their igneous age (if the sample was dated) or to the age attributed to the igneous
200 unit from which the sample has been taken (see Figure 2 for sampling location and appendix
201 C3). All the samples are subalkaline, dioritic to granitic in composition (SiO_2: 57.1 – 77.8 wt%
202 and [Na_2O+K_2O]: 3.9 – 11.5 wt%; Fig. 5) and plot predominantly in the low K calc-alkaline
203 series (< 3 wt% K_2O; low FeO/MgO ratios). Only 7 samples show high K contents, including
204 one with an abnormal K_2O value (7.5 wt%) probably related to post-magmatic alteration. All
205 the samples have high Mg# (>30; Mg# = Mg/[Fe+Mg] * 100; Mg-number) which tend to
206 decrease with increasing SiO_2 content and form a magmatic trend of magnesian diorites,
207 granodiorites, granites and leucogranites according to the Frost and Frost (2008)
208 classification. There is no systematic variation in major element compositions in function of
209 their crystallization age. As a whole, based on their major element signatures, those samples
210 are comparable to the felsic rocks found in the Kohistan oceanic arc (Jagoutz et al., 2009).
211 The MORB-normalized spider diagrams for each magmatic pulse described in the previous
212 section are showed on Figure 5. Evolved magmatic rocks emplaced during the first magmatic
213 pulse (730 - 760 Ma, group 1) have typical arc signature with enrichment in LILE (Rb, Ba, Sr)
214 compared to HFSE, negative Nb-Ta anomalies, positive Pb anomalies, low La/Yb and Sr/Y
215 (from 2 to 8 and ranging between 7 and 31, respectively) with HREE and Y MORB-normalized

contents between 1 and 0.1 (Fig. 5a). Granitoids from the second magmatic pulse (690-710 Ma, group 2) display similar patterns but some samples show severe depletion in HREE leading to globally higher La/Yb ratios (2 to 25) and Sr/Y (9 to 1420). Samples with the highest La/Yb ratios display strong positive anomalies in Sr and Eu reflecting either plagioclase accumulation or melting of a plagioclase-bearing assemblage (Fig. 5b). The younger group (660-640 Ma, group 3) is characterized by a dominant subset of samples having the same trace-element pattern as the arc rocks from the group 1 (760-730 Ma). Another subset is marked by strongly Y- and HREE-depleted patterns comparable to arc rocks from the group 2 (Fig. 5c).

Additionally, some felsic samples are characterized by very high La/Yb and Sr/Y ratios (ranging from 2 to 45 and 13 to 660, respectively) associated with pronounced positive peaks in Sr, Eu and Zr. These HREE-depleted leucogranites belonging to group 2 and 3 are often found as leucosomes in anatectic domains within the Sirwa and Bou Azzer complexes and are interpreted as the product of partial melting of a plagioclase-bearing mafic precursor in the garnet stability field (Triantafyllou et al., 2016; 2018).

3.3 Isotopic signatures of magmatic pulses

$^{143}Nd/^{144}Nd$ data were determined by MC-ICPMS on 32 samples (see appendix A2 for detailed protocol and instruments used) and were compared to results from twenty-eight samples reported in the literature (Mrini, 1993; Beraaouz et al., 2004; D'Lemos et al., 2006; Triantafyllou et al., 2018). Initial □Nd values (□Nd_t) were calculated using the available U-Pb zircon ages (as either direct or indirect dating; see summary of isotopic data and considered U-Pb ages in appendix table C2). The □Nd_t of the Moroccan paleo-arc rocks show positive values ranging between +2.7 and +10.1 with a median at +5.9. Median values for each magmatic pulse slightly decrease through time, essentially between group 1 (760-730 Ma) at +7.1 and group 2-3 (710-690 Ma) at +5.4 and (660-640 Ma) at +5.7, respectively. These values are close to the signature of contemporary depleted mantle (□Nd_t of +6.5 at 700 Ma based on the depleted mantle model of DePaolo, 1981) and together with their subduction geochemical fingerprint,

244 are consistent with their emplacement in an arc setting. The general isotopic composition of
245 the Moroccan arc reflects a large input of new mantle-derived material without substantial
246 assimilation by the West African Craton Paleoproterozoic crustal basement defined by highly
247 negative □Nd (ranging between -0.4 and -17.2 with weighted mean at -8.2; Ennih and Liégeois,
248 2008).
249

250 ## 4. Discussion

251 ### *4.1 Arc crust thickening recorded by geochemical proxies*

252 Crustal thickness of arcs can be qualitatively estimated by key geochemical proxies such as
253 Sr/Y and La/Yb ratios (Profeta et al., 2015). This method is based on the very different behavior
254 of these elements with respect to pressure conditions during igneous processes occurring in
255 arc crust. At pressure exceeding 8-10 kbar, garnet (± amphibole and pyroxene) is stable in the
256 solid residue after either partial melting of mafic rocks or fractional crystallization and extraction
257 of mafic to intermediate melts; while at lower pressure, plagioclase (± amphibole and
258 pyroxene) replaces garnet in both cases (Lopez and Castro, 2001; Alonso-Perez et al., 2009;
259 Müntener and Ulmer, 2018; Palin et al., 2016). Sr and La partition preferentially into the
260 plagioclase-bearing solid residues producing intermediate to felsic melts with low Sr/Y and
261 La/Yb ratios. At higher pressure, Y and Yb are preferentially incorporated into garnet-bearing
262 residues and, consequently, melts formed in the stability field of garnet in the lower crust of
263 thick arcs display high Sr/Y and La/Yb ratios (Chapman et al., 2015).
264 Intermediate to felsic arc rocks emplaced during the first magmatic episode (group 1: 730-760
265 Ma) in the Moroccan arc form a typical calc-alkaline Andesite-Dacite-Rhyolite (ADR) arc suite
266 marked by low $[La/Yb]_N$ and Sr/Y ratios ($_N$: normalized to chondrite composition; Fig. 7). This
267 chemical signature characterizes evolved rocks produced in oceanic arc settings but more
268 particularly, immature and thin arc sections like the Scotia arc for example (Leat et al., 2007).
269 The parental melt of these evolved rocks formed by fractional crystallization or partial melting
270 in the presence of plagioclase and absence of garnet in the solid residue, *i.e.* below 8-10 kbar

271 corresponding to a maximum crustal depth of 30-35 km (Fig. 7: model C). Evolved arc rocks
272 formed during the second and third magmatic episodes (group 2 and 3: 690-710 Ma and 640-
273 660 Ma, respectively) similarly display low $[La/Yb]_N$ and Sr/Y values but numerous samples
274 show higher values by one or two orders of magnitude (Fig. 7). These signatures are
275 consistent with fractional melting trends and/or crystallization models of a hydrous mafic
276 source in the stability field of garnet (models A and B in Fig. 7; see appendix C4 for fractional
277 melting model parameters and the composition of residual melt produced by fractional
278 crystallization). The occurrence of garnetite and garnet-bearing leucosomes within contact
279 reaction zones surrounding small hornblende-gabbroic and hornblenditic intrusions suggests
280 that garnet was a product of dehydration and dehydration melting reactions within the
281 Moroccan arc crust (Triantafyllou et al., 2016; 2018). The stability of garnet in the source of
282 these melts implies that they formed at a minimum pressure of 10 kbar corresponding to crustal
283 depth exceeding 35 km. These geochemical signatures mimic adakitic to dacitic lava produced
284 in modern mature and thick oceanic arcs, like the Aleutian arc (Moho depth reaching >50 km;
285 Calvert and McGeary, 2013) and in thick continental arcs (up to 70 km in the Andes; Beck et
286 al., 1996) (see grey symbols in Fig. 7). The composition of HREE- and Y-depleted intermediate
287 and evolved rocks that formed during the second and third magmatic events in the Moroccan
288 arc also resembles that of trondhjemitic melts produced by dehydration melting in the root of
289 thick Phanerozoic and Neoproterozoic accreted oceanic arcs (see blue symbols in Fig. 7;
290 Garrido et al., 2006; Berger et al., 2011). Based on the evolution of Sr/Y and La/Yb ratios, we
291 argue that the magmatic activity of the Moroccan arc recorded important crustal thickening,
292 particularly between the first and second magmatic events, *i.e*. between 730 and 710 Ma (Fig.
293 7). The evolved magmatic rocks emplaced during the second pulse show a relatively uniform
294 spread of HREE and Y (Fig. 5b and Fig. 7) suggesting that the magma genesis and its
295 chemical diversification occurred at different levels of the arc crust from lower to middle crust.
296 In turn, arc rocks formed during the third magmatic event show a bimodal distribution (Fig. 5c
297 and Fig. 7) suggesting two distinct sources and/or depths of differentiation: a first subset
298 formed under garnet stability field (with average HREE and Y contents), with a composition

similar to arc rocks emplaced during first magmatic episode and a second one in presence of garnet (HREE- and Y-depleted), hence reflecting a deeper crustal source. The latter indicates that the arc crust maintained a minimum thickness of 35 km during the third magmatic pulse before its tectonic obduction onto the continental margin.

4.2 Crustal thickening triggered by magmatic accretion and tectonic shortening

Crustal thickening in arc systems can be caused by two mechanisms: *(i)* addition of mantle-derived magma into the arc crust or *(ii)* compressional/shortening tectonics affecting the upper plate of the subduction system. Although upper plate shortening is rare in active oceanic arcs, it does characterize continental arcs such as the Central Andean section (Haschke et al., 2006) and the evolution of fossil continental arc complexes in the Coast Belt of the NW Cordillera (e.g., Miller and Paterson, 2001). In our case study, the first magmatic event (760-730 Ma) is concomitant with back-arc spreading and the formation of a supra-subduction zone ophiolite, attesting that the overriding plate was initially in an extensional regime most likely in response to a steep subducting slab as in most modern island arcs (Syracuse and Ambers, 2006). A major deformation event occurred between the first and second magmatic episodes and marked a tectonic inversion from extensional to compressional. This major deformation event is constrained between 730 and 710 Ma as it only affected the arc rocks emplaced during the first magmatic pulse (760-730 Ma; Triantafyllou et al., 2018). Two observations support crust thickening as a result of tectonic activity during this 730-710 Ma timespan: *(i)* burial of the 760-730 Ma meta-andesitic rocks to >20 km depth (Triantafyllou et al., 2016) and *(ii)* stacking of the 762 Ma back-arc ophiolite onto the 750-730 Ma arc rocks followed by the intrusion of 660-640 Ma mafic to felsic magmas into the stacked units (Hefferan et al., 2014; Triantafyllou et al., 2016, 2018; Inglis et al. 2017; Fig. 2b).

Such tectonically-driven crustal thickening has not been observed yet in modern intra-oceanic arc systems which in contrast, are associated with extensional (e.g., Bonin, Mariana, Tonga, Kermadec, Scotia, Lesser Antilles island arcs) or neutral tectonic regime in the overriding plate (e.g., Aleutian oceanic arc; Leat and Larter, 2003). Furthermore, modern oceanic arcs are

relatively short-lived (e.g., the Aleutian arc is 46 - 75 Ma old; Jicha and Jagoutz, 2015 and references therein) and thus, show limited possibilities for changes in their intra-arc tectonic regimes. Analogue and numerical geodynamic models showed that, for long-lived subduction systems, the tectonic regime in the overriding crust can significantly change through time, alternating between extensional and compressional during the evolution of a single subduction system (e.g., Clark et al., 2008; Guillaume et al., 2009). Compressional regime into the upper plate – and the arc system itself – requires a rheological coupling between the subducting slab and the overriding lithosphere. The efficiency of plates coupling can be influenced by the amount of fluids and melts in the overriding lithospheric section (Billen, 2008; Nikolaeva et al., 2008; Sizova et al., 2010; Baitsch et al, 2014), relative velocities of the subducting and overriding plates (Arcay et al., 2008), variations of slab geometry due to subduction of buoyant crustal elements (active ridge, seamounts, oceanic plateau; Mason et al., 2010) and/or to deep anchoring of the subducting slab (Heuret and Lallemand, 2005; Guillaume et al., 2009).

Compressional tectonics in the upper plate of subduction zone have also been recognized in a few modern oceanic arcs formed in complex geodynamic contexts. In intra-oceanic settings, Philippines, Luzon and Ryukyu arcs are atypical as they were built on pre-existing island arcs and ophiolitic remnants (Pubellier et al., 1996). These oceanic arcs are characterized by specific plates kinematic conditions which induce compressional (shortening) regime in their respective upper plates (Lallemand et al., 2008). Other case studies refer to ‘transitional arc systems’ between continental and intra-oceanic arc endmembers (Ducea et al., 2015b), which include Japan, New Britain, New Hebrides and Solomon arcs (e.g., Petterson et al., 1999; Okada and Ikeda, 2012). In comparison to intra-oceanic settings, these transitional arcs can have a long-lived magmatic evolution. They generally evolve at a certain geographic proximity to the continental margin but may remain oceanic in nature as they form on extended continental passive margins made of time-integrated accumulations of accreted terranes including oceanic plateaus and/or arc magmatic products (Ducea et al., 2015b). In such context, a compressional regime can be induced in the oceanic arc *sensu stricto* due to its docking and tectonic accretion on this transitional margin. Shortening is transferred by the

indirect (through buoyant oceanic terranes) collision between the oceanic arc and the continental margin. Amongst other examples, the evolution of the Solomon oceanic arc is thought to be an illustration of such mechanisms for which accretionary processes and associated compressional regime ultimately led to a flip in subduction polarity (Petterson et al., 1999).

We propose that the Moroccan arc underwent a similar long-lived evolution typical of such transitional arc settings. This geodynamic scenario would also be consistent with the isotopic signature of the second magmatic pulse (Fig. 6), precluding a significant contribution of the continental radiogenic old crust margin into its arc magmatic source; neither through the subduction of eroded products or as subduction of the continental margin itself nor through the formation of an Andean-type continental arc system. Our integrative study rather suggests that the major deformation event recorded in the older portion of the Moroccan oceanic arc resulted from a soft-accretion or soft-docking of the primary arc. Such a scenario could account for tectonic shortening in an oceanic domain and induced crustal thickening within a relatively short time span.

4.3 Linking episodic magmatism, crustal thickening and tectonic regime in oceanic arcs

We argue that the magmatic activity in the Neoproterozoic Moroccan oceanic arc was episodic, alternating three successive magmatic pulses with relatively short periods of magmatic lull (20-30 Myr; Fig. 4). Such a non-steady state evolution is very similar to the magmatic arc *tempo* which characterizes the evolution of several long-lived accreted and active continental arcs (e.g., western North American arc, the central Andes, the Gangdese arc in southern Tibet and the Taknar arc complex in NE Iran; respectively studied by e.g., Armstrong, 1988; Ducea and Barton, 2007; Ma et al., 2015; Moghadam et al., 2017). However, this process is very atypical for oceanic arc systems where magmatic production appears to be continuous in modern and Phanerozoic records (Hacker et al., 2008; Rioux et al., 2010; Bosch et al., 2011; see Fig. 3 in Paterson and Ducea, 2015). The causes of magmatic shutdowns during the evolution of

ocean-ocean subduction zone are still not explored. We propose here a conceptual model based on field, geochemical and petrological evidences of the Moroccan oceanic arc remnant: *The first magmatic shutdown* of the Moroccan arc is constrained between 730 and 710 Ma, concurrently to a tectonic shortening event and associated crustal thickening described in the previous section. This suggests a strong interplay between subduction-induced tectonics, crustal thickening and production rate of arc magma. The onset of the magmatic history in the Moroccan oceanic arc is marked by high melt productivity, which is typically observed in Cordilleran subduction systems (Ducea et al., 2017). For the Moroccan case study, it is most likely due to the temporary steepening of the slab which is evidenced by back-arc spreading in the overriding crust and the development of a 762 and 742 Ma aged oceanic crust (respectively, Samson et al., 2004; Triantafyllou et al., *in prep*.). The compressional regime and thickening of the arc crust suggest that a tectonic inversion occurred in the upper plate, synchronously to a quiescence of magmatic activity. Then, the second magmatic event occurred between 710 and 680 Ma producing evolved arc rocks with the typical chemical signature of mature arc systems and intruding preexisting structures including stacked arc-related units. Important arc crust thickening can be responsible for magmatic shutdown by freezing the mantle wedge corner flow (DeCelles et al., 2009); as shown in North America where magmatic flare-ups follow major events of retro arc shortening by about 15–25 Myr (DeCelles, 2004). Such a model brings a consensual approach to link magmatic shutdown, tectonic shortening and crustal thickening observed in the Moroccan oceanic arc and supports that the mechanisms controlling the evolution of continental arcs can be applied to long-lived intra-oceanic systems. Another potential scenario would consider geodynamic causes that are external to the evolution of the magmatic arc system, including plate reconfiguration and accretionary/collisional processes. In this perspective, the first magmatic shutdown of the Moroccan arc could be a consequence of the transition of the arc system from an intra-oceanic to a transitional geodynamic setting subsequent to soft-docking of the primary arc on a buoyant composite continental margin (see section 4.2). Such soft-docking scenario would require an initial ocean-wards subduction polarity leading to arc accretion/docking after full consumption

409 of the subducted oceanic crust. Then, continent-wards subduction would be re-initiated after
410 flipping in subduction polarity. The arc could still evolve in such a steady state for a long period
411 up to the ultimate closure of the oceanic domain. Polarity flip during subduction has been
412 proposed for several modern oceanic arcs in SW Pacific (e.g., Solomon, New Hebrides, New
413 Guinea arcs; Cooper and Taylor, 1987; Meffre and Crawford, 2001; Boutelier and Chemenda,
414 2011) which could lead to complex polyphased structures similar to that in the Moroccan arc
415 after their tectonic obduction on a continental margin.
416 *The second magmatic lull* is constrained between 680 and 660 Ma during the evolution of the
417 Moroccan arc. This second magmatic shutdown is different from the first one as arc rocks
418 emplaced during both the second and third magmatic pulses are undeformed. This prevented
419 any major tectonic event during the cessation of magmatic activity and suggests a relatively
420 steady-state evolution of the subduction from 710 Ma. Nd isotopic signature of arc rocks
421 emplaced during the second and third magmatic pulses are indiscernible from each other (Fig.
422 6) suggesting no rejuvenation of the sub-arc mantle composition. The Moroccan arc crust was
423 particularly thick during the second event (> 35 km) and evolved arc magmas were mainly
424 produced during this episode by partial melting in the middle to lower crust of the arc
425 (Triantafyllou et al., 2018). In such thickened arc frameworks, magmatic shutdown could
426 mainly result from two mechanisms: *(i)* Thickened arc crust can induce filtration and
427 accumulation of primary mafic magma into lower crustal reservoirs (Dufek and Bergantz 2005).
428 This process can temporarily lead to a decrease in magmatic productivity within the middle
429 and upper crust and ultimately, flare up in large batholith-forming episodes (DeCelles et al.
430 2009). However, this scenario is less in agreement with the bimodal distribution of the
431 composition of the arc magma produced during the third magmatic pulse (660-640 Ma).
432 Alternatively, *(ii)* this second magmatic shutdown could be caused by the critical thickening
433 reached by the arc crust due to new addition of magmatic rocks during the second magmatic
434 episode and, as mentioned above, the freezing of the mantle wedge-derived influx. The third
435 magmatic episode would then be triggered by the delamination of the dense arc root and
436 subsequent reactivation of the mantle wedge dynamics and related magmatism. This scenario

437 is preferred for explaining the last stage of the Moroccan oceanic arc. Magmatism would be
438 derived from partial melts of the garnet-bearing arc root as it underwent higher temperature
439 conditions during foundering (HREE- and Y-depleted signature; Fig. 5c) as well as from high
440 proportion of dioritic and granodioritic magma emplaced after lower crust delamination, hence,
441 in a thinner arc crust setting (HREE- and Y-non-depleted signature; Fig. 5c). Nevertheless,
442 this second part of the evolution of the Moroccan arc requires further petrochronological
443 investigation to better constrain the cause and timing of this short period of magmatic
444 quiescence.
445

446 **Concluding remarks**

447 The Moroccan arc remnants are the products of a long-lived (100-120 Myr) Neoproterozoic
448 subduction system. Based on U-Pb age distribution and detailed geological mapping of each
449 arc unit, we infer that the magmatic evolution of the arc was episodic, characterized by three
450 successive pulses cadenced each 40-50 Myr and interspersed by short periods of magmatic
451 silence. Shortening tectonics in the upper plate of the subduction is concomitant with the first
452 magmatic shutdown (730-710 Ma) resulting in back-arc thrusting onto the arc flank. Soft-
453 docking of the oceanic arc on a buoyant, extended continental margin is invoked to explain
454 shutdown of magmatism, crustal thickening and inversion of the tectonic regime. The second
455 magmatic shutdown (680-660 Ma) is likely caused by critical arc crust thickening which froze
456 the subarc mantle flux. The third magmatic episode is marked by a bimodal chemical signature
457 of intermediate magmatic products suggesting that magmatism was triggered by the
458 delamination of the dense root of the oceanic arc.
459 Arc growth driven by both rhythmic magmatism and tectonic shortening is usually a fingerprint
460 of modern continental arcs, but our results emphasize that it could also characterize long-lived
461 oceanic arcs, at least during the Late Neoproterozoic. These findings call for further
462 investigations on the timing of magmatic activity in oceanic arcs. While their continental
463 counterparts have been well studied, mapped and covered by U-Pb geochronology due to the

abundance of intermediate to felsic rocks (easily datable by zircon geochronology), magmatic tempo of oceanic arcs is still under-investigated. Future research should explore geochronological systems adapted for mafic rocks (U-Pb dating on baddeleyite, rutile, titanite, apatite), as zircon-bearing intermediate to felsic rocks are less common in oceanic environments. Moreover, future sampling should focus not only on igneous rocks forming the arcs but also on the detrital sedimentary rocks that accumulated in forearc or back-arc basins and were sourced from the erosion of former volcanic/plutonic arc rocks. This strategy applied to active arcs and coupled with detailed geochronological studies on accreted island arc sections will help understanding if rhythmic magmatism in oceanic arcs is restricted to Neoproterozoic geodynamics or is a feature of long-lived oceanic subductions zones regardless of their age.

Acknowledgements

The first author (AT) thanks the Rotary Club de Mons and the University of Mons for providing their financial support via the Pierre Jacobs post-doctoral grant (2018). AT is a FRS-FNRS post-doctoral research fellow for the PROBARC project (Grant CR n°1.B.414.20F). We would also like to thank Wendy Debouge and Jeroen de Jong from the GTime laboratory (ULB) for their help in samples preparation and for acquiring Nd isotopic data. M.N.D. acknowledges support from US National Science Foundation grant EAR 1725002 and the Romanian Executive Agency for Higher Education, Research, Development and Innovation Funding projects PN-III-P4-ID-PCE-2016-0127 and PN-III-P4-ID-PCCF-2016-0014. The authors also thank one anonymous reviewer and K. Hefferan for their constructive reviews along with the Precambrian Research editorial board for their handling of the present manuscript.

Data availability

All data used in this manuscript are available in the appendices. Further queries and information requests should be directed to the lead authors A.T. (antoinetri@gmail.com).

Appendices

A. Analytical methods

A1. Whole rock major and trace elements analysis

Major and trace elements have been determined on bulk samples either by X-Ray Fluorescence (XRF) and Laser-Ablation Inductively Coupled Plasma Mass-Spectrometer (LA-ICP-MS) on fused beads at the ICP-MS Laboratory of Central Analytical Facilities (CAF; Stellenbosch University, South Africa). Glass beads were prepared for XRF analysis using 7 g of high purity trace element and Rare Earth Element-free flux ($LiBO_2$ = 32.83%, $Li_2B_4O_7$ = 66.67%, LiI = 0.50%) mixed with 0.7 g of the powder sample in a platinum crucible. The concentration of the control standards that were used in the calibration procedures for major element analysis fits the range of concentration of the samples. Amongst these standards were NIM-G (Granite from the Council for Mineral Technology, South Africa) and BE-N (Basalt from the International Working Group). Trace elements on bulk samples have been analyzed using the analytical procedure described in Eggins (2003). Fusion disks prepared for XRF analysis were coarsely crushed and a chip of each sample was mounted in a round resin disk for analysis using Laser Ablation ICP-MS with a Resolution 193 nm Excimer laser from ASI connected to an Agilent 7700 ICP-MS. Two spots of 100 µm were ablated on each sample using a frequency of 10 Hz and a fluence of ~6 J/cm2. NIST 610 glass (values from Jochum et al., 2011) was used for quantification and analyzed every 15 samples, along with BCR-2G & BHVO-2G (values from GeoReM: Jochum et al., 2005). A fusion control standard from certified basaltic reference material (BCR-2, and BHVO-1, values from Jochum et al., 2016) is also analyzed in the beginning of a sequence to verify the effective ablation of fused material. LA-ICP-MS data was processed using Glitter v4.4.4 software (Access Macquarie Ltd., Macquarie University NSW 2109). Geochemical data can be found in Table C3 (see Günther et al., 2001 for more details about detection limits and calibration procedure).

A2. Nd isotopic analyses

Rock powders were dissolved in a concentrated HNO_3/HF mixture (3/1) followed by HCl digestion. Nd was isolated from the matrix using a two-column ion-exchange chromatography technique following the method described in Debaille et al. (2013). The ^{143}Nd samples were measured using a high-resolution Nu Instruments Plasma I MC-ICPMS at the Laboratoire G-Time (ULB). The isotopic ratios were measured by static multi-collection in dry plasma with an Aridus II desolvator. For ^{143}Nd each analysis consists of 3 blocks of 20 runs each. The repeated measurements of Rennes international standard gave an external reproducibility of 14 ppm (2sigma, n=5). Neodymium isotopic compositions were corrected by sample-standard bracketing using the recommended value of the Rennes standard ($^{143}Nd/^{144}Nd$=0.511961; Chauvel and Blichert-Toft, 2001).

B. Supplementary materials

Interactive location maps (created using Geolokit software; Triantafyllou et al., 2017):

- B1. U-Pb geochronological data (B1_Map_MagmaticAges.kmz)
- B2. Nd isotopic data of Moroccan paleo-arc rocks (B2_Map_Nd_IsotopicData.kmz)

C. Data tables

- *C1. U-Pb geochronological data (Appendix_C1_MagmaticAges.pdf).*
- *C2. Nd isotopic data of Moroccan paleo-arc rocks (Appendix_C2_Nd_isotopic_analyses.pdf).*
- *C3. Major and trace elements composition of Moroccan arc rocks (Appendix_C3_Geochemical_analyses.pdf).*
- *C4. REE modelling: fractional melting and crystallization parameters (Appendix_C4_Models_FractionalMelting-Crystallization.xlsx).*

References cited

Admou, H., Razin, P., Egal, E., Youbi, N., Soulaimani, A., Blein, O., & Anzar, C. (2013). Notice explicative de la Carte géologiques du Maroc (1/50 000), feuille Aït Ahmane. *Notes et Mémoires du service Géologique du Maroc*, (533 bis), carte.

Ahmed, A. H., Arai, S., Abdel-Aziz, Y. M., & Rahimi, A. (2005). Spinel composition as a petrogenetic indicator of the mantle section in the Neoproterozoic Bou Azzer ophiolite, Anti-Atlas, Morocco. *Precambrian Research*, *138*(3-4), 225-234.

Alonso-Perez, R., Müntener, O., & Ulmer, P. (2009). Igneous garnet and amphibole fractionation in the roots of island arcs: experimental constraints on andesitic liquids. *Contributions to Mineralogy and Petrology*, *157*(4), 541.

Arcay, D., Lallemand, S., & Doin, M. P. (2008). Back-arc strain in subduction zones: Statistical observations versus numerical modeling. Geochemistry, Geophysics, Geosystems, 9(5).

Armstrong RL (1988) Mesozoic and early Cenozoic magmatic evolution of the Canadian Cordillera. Geological Society of America Special Paper 218: 55-91

Baitsch-Ghirardello, B., Gerya, T. V., & Burg, J. P. (2014). Geodynamic regimes of intra-oceanic subduction: Implications for arc extension vs. shortening processes. Gondwana Research, 25(2), 546-560.

LeBas, M. L., Maitre, R. L., Streckeisen, A., Zanettin, B., & IUGS Subcommission on the Systematics of Igneous Rocks. (1986). A chemical classification of volcanic rocks based on the total alkali-silica diagram. Journal of petrology, 27(3), 745-750.

Beck, S. L., Zandt, G., Myers, S. C., Wallace, T. C., Silver, P. G., & Drake, L. (1996). Crustal-thickness variations in the central Andes. Geology, 24(5), 407-410.

Beraaouz, E. H., Ikenne, M., Mortaji, A., Madi, A., Lahmam, M., & Gasquet, D. (2004). Neoproterozoic granitoids associated with the Bou-Azzer ophiolitic melange (Anti-Atlas, Morocco): evidence of adakitic magmatism in an arc segment at the NW edge of the West-African craton. *Journal of African Earth Sciences*, *39*(3-5), 285-293.

Berger, J., Caby, R., Liégeois, J. P., Mercier, J. C. C., & Demaiffe, D. (2011). Deep inside a Neoproterozoic intra-oceanic arc: growth, differentiation and exhumation of the Amalaoulaou complex (Gourma, Mali). *Contributions to Mineralogy and Petrology*, *162*(4), 773-796.

Billen, M. I. (2008). Modeling the dynamics of subducting slabs. Annu. Rev. Earth Planet. Sci., 36, 325-356.

Blein, O., Baudin, T., Chevremont, P., Soulaimani, A., Admou, H., Gasquet, P., A. Cocherie, E. Egal, N. Youbi, P. Razin, M. Bouabdelli & P. Gombert (2014). Geochronological constraints on the polycyclic magmatism in the Bou Azzer-El Graara inlier (central Anti-Atlas Morocco). *Journal of African Earth Sciences*, *99*, 287-306.

Bodinier, J.L., Dupuy, C., Dostal, J., (1984). Geochemistry of precambrian ophiolites from Bou Azzer, Morocco. Contrib. Miner. Petrol. 78, 43–50.

Bosch, D., Garrido, C. J., Bruguier, O., Dhuime, B., Bodinier, J. L., Padròn-Navarta, J. A., & Galland, B. (2011). Building an island-arc crustal section: time constraints from a LA-ICP-MS zircon study. *Earth and Planetary Science Letters*, *309*(3-4), 268-279.

584 Bousquet, R., El Mamoun, R., Saddiqi, O., Goffé, B., Möller, A., & Madi, A. (2008). Mélanges and
585 ophiolites during the Pan-African orogeny: the case of the Bou-Azzer ophiolite suite
586 (Morocco). *Geological Society, London, Special Publications*, *297*(1), 233-247.
587 Boutelier, D., & Chemenda, A. (2011). Physical Modeling of Arc–Continent Collision: A Review of 2D,
588 3D, Purely Mechanical and Thermo-Mechanical Experimental Models. In *Arc-continent collision* (pp.
589 445-473). Springer, Berlin, Heidelberg.
590 Calvert, A. J., & McGeary, S. E. (2013). Seismic reflection imaging of ultradeep roots beneath the
591 eastern Aleutian island arc. Geology, 41(2), 203-206.
592 Chapman JB, Ducea MN, DeCelles PG, Profeta L (2015) Tracking changes in crustal thickness during
593 orogenic evolution with Sr/Y: an example from the North American Cordillera. Geology 43: 919-922.
594 Chauvel, C., & Blichert-Toft, J. (2001). A hafnium isotope and trace element perspective on melting of
595 the depleted mantle. Earth and Planetary Science Letters, 190(3-4), 137-151.
596 Clark, S.R., Stegman, D., Müller, R.D., (2008). Episodicity in back-arc tectonic regimes. Physics of
597 The Earth and Planetary Interiors 171 (1–4), 265–279.
598 Cooper, P., & Taylor, B. (1987). Seismotectonics of New Guinea: A model for arc reversal following
599 arc-continent collision. *Tectonics*, *6*(1), 53-67.
600 Currie, C. A., Ducea, M. N., DeCelles, P. G., & Beaumont, C. (2015). Geodynamic models of
601 Cordilleran orogens: Gravitational instability of magmatic arc roots. *Geodynamics of a Cordilleran*
602 *Orogenic System: The Central Andes of Argentina and Northern Chile: Geological Society of America*
603 *Memoir*, *212*, 1-22.
604 D'Lemos, R. S., Inglis, J. D., & Samson, S. D. (2006). A newly discovered orogenic event in Morocco:
605 Neoproterozoic ages for supposed Eburnean basement of the Bou Azzer inlier, Anti-Atlas
606 Mountains. *Precambrian Research*, *147*(1-2), 65-78.
607 Debaille, V., O'Neill, C., Brandon, A. D., Haenecour, P., Yin, Q. Z., Mattielli, N., & Treiman, A. H. (2013).
608 Stagnant-lid tectonics in early Earth revealed by 142Nd variations in Late Archean rocks. Earth and
609 Planetary Science Letters, 373, 83-92.
610 DeCelles, P. G., Ducea, M. N., Kapp, P., & Zandt, G. (2009). Cyclicity in Cordilleran orogenic
611 systems. *Nature Geoscience*, *2*(4), 251.
612 DeCelles, P.G., 2004, Late Jurassic to Eocene evolution of the Cordilleran thrust belt and foreland
613 basin systems, western U.S.A: American Journal of Science, v. 304 pp. 105-168 doi:
614 10.2475/ajs.304.2.105.
615 DePaolo, D. J. (1981). A neodymium and strontium isotopic study of the Mesozoic calc-alkaline granitic
616 batholiths of the Sierra Nevada and Peninsular Ranges, California. *Journal of Geophysical Research:*
617 *Solid Earth*, *86*(B11), 10470-10488.
618 Ducea, M. (2001). The California arc: Thick granitic batholiths, eclogitic residues, lithospheric-scale
619 thrusting, and magmatic flare-ups. GSA today, 11(11), 4-10.
620 Ducea, M. N., & Barton, M. D. (2007). Igniting flare-up events in Cordilleran arcs. *Geology*, *35*(11),
621 1047-1050
622 Ducea, M. N., Bergantz, G. W., Crowley, J. L., & Otamendi, J. (2017). Ultrafast magmatic buildup and
623 diversification to produce continental crust during subduction. *Geology*, *45*(3), 235-238.

624 Ducea, M. N., Paterson, S. R., & DeCelles, P. G. (2015). High-volume magmatic events in subduction
625 systems. *Elements*, *11*(2), 99-104.
626 Ducea, M. N., Saleeby, J. B., & Bergantz, G. (2015). The architecture, chemistry, and evolution of
627 continental magmatic arcs. *Annual Review of Earth and Planetary Sciences*, *43*, 299-331.
628 Dufek, J., & Bergantz, G. W. (2005). Lower crustal magma genesis and preservation: a stochastic
629 framework for the evaluation of basalt–crust interaction. *Journal of Petrology*, *46*(11), 2167-2195.
630 Eggins, S. M. (2003). Laser ablation ICP-MS analysis of geological materials prepared as lithium borate
631 glasses. Geostandards Newsletter, 27(2), 147-162.
632 El Hadi, H., Simancas, J. F., Martínez-Poyatos, D., Azor, A., Tahiri, A., Montero, P., C.M. Fanning,
633 F.Bead & González-Lodeiro, F. (2010). Structural and geochronological constraints on the evolution of
634 the Bou Azzer Neoproterozoic ophiolite (Anti-Atlas, Morocco). *Precambrian Research*, *182*(1-2), 1-14.
635 Ennih, N., & Liégeois, J. P. (2008). The boundaries of the West African craton, with special reference
636 to the basement of the Moroccan metacratonic Anti-Atlas belt. *Geological Society, London, Special*
637 *Publications*, *297*(1), 1-17.
638 Errami, E., Bonin, B., Laduron, D., & Lasri, L. (2009). Petrology and geodynamic significance of the
639 post-collisional Pan-African magmatism in the Eastern Saghro area (Anti-Atlas, Morocco). *Journal of*
640 *African Earth Sciences*, *55*(1-2), 105-124.
641 Frost, B. R. and Frost, C. D. (2008). A geochemical classification for feldspathic igneous rocks. *Journal*
642 *of Petrology*, *49*(11), 1955-1969.
643 Ganade de Araujo, C. E., Weinberg, R. F., & Cordani, U. G. (2014). Extruding the Borborema Province
644 (NE-Brazil): a two-stage Neoproterozoic collision process. *Terra Nova*, *26*(2), 157-168.
645 Garrido, C. J., Bodinier, J. L., Burg, J. P., Zeilinger, G., Hussain, S. S., Dawood, H., & Gervilla, F.
646 (2006). Petrogenesis of mafic garnet granulite in the lower crust of the Kohistan paleo-arc complex
647 (Northern Pakistan): implications for intra-crustal differentiation of island arcs and generation of
648 continental crust. *Journal of Petrology*, *47*(10), 1873-1914.
649 Gasquet, D., Levresse, G., Cheilletz, A., Azizi-Samir, M. R., & Mouttaqi, A. (2005). Contribution to a
650 geodynamic reconstruction of the Anti-Atlas (Morocco) during Pan-African times with the emphasis on
651 inversion tectonics and metallogenic activity at the Precambrian–Cambrian transition. *Precambrian*
652 *Research*, *140*(3-4), 157-182.
653 Gasquet, D., Ennih, N., Liégeois, J. P., Soulaimani, A., & Michard, A. (2008). The pan-african belt.
654 In *Continental evolution: the geology of Morocco* (pp. 33-64). Springer, Berlin, Heidelberg.
655 Gerya, T. V. (2011). Intra-oceanic subduction zones. In Arc-continent collision (pp. 23-51). Springer,
656 Berlin, Heidelberg.
657 Gorczyk, W., Willner, A. P., Gerya, T. V., Connolly, J. A., & Burg, J. P. (2007). Physical controls of
658 magmatic productivity at Pacific-type convergent margins: Numerical modelling. *Physics of the Earth*
659 *and Planetary Interiors*, *163*(1-4), 209-232.
660 Guillaume, B., Martinod, J., & Espurt, N. (2009). Variations of slab dip and overriding plate tectonics
661 during subduction: Insights from analogue modelling. *Tectonophysics*, *463*(1-4), 167-174.

662 Günther, D., Quadt, A. V., Wirz, R., Cousin, H., & Dietrich, V. J. (2001). Elemental analyses using laser
663 ablation-inductively coupled plasma-mass spectrometry (LA-ICP-MS) of geological samples fused with
664 Li 2 B 4 O 7 and calibrated without matrix-matched standards. Microchimica Acta, 136(3-4), 101-107.
665 Hacker, B. R., Mehl, L., Kelemen, P. B., Rioux, M., Behn, M. D., & Luffi, P. (2008). Reconstruction of
666 the Talkeetna intraoceanic arc of Alaska through thermobarometry. *Journal of Geophysical Research:*
667 *Solid Earth*, *113*(B3).
668 Hacker, B. R., Kelemen, P. B., Rioux, M., McWilliams, M. O., Gans, P. B., Reiners, P. W., & Vervoort,
669 J. D. (2011). Thermochronology of the Talkeetna intraoceanic arc of Alaska: Ar/Ar, U-Th/He, Sm-Nd,
670 and Lu-Hf dating. *Tectonics*, *30*(1).
671 Haschke, M., Günther, A., Melnick, D., Echtler, H., Reutter, K. J., Scheuber, E., & Oncken, O. (2006).
672 Central and southern Andean tectonic evolution inferred from arc magmatism. In The Andes (pp. 337-
673 353). Springer, Berlin, Heidelberg.
674 Hefferan, K., Soulaimani, A., Samson, S. D., Admou, H., Inglis, J., Saquaque, A., Chaib Latifa &
675 Heywood, N. (2014). A reconsideration of Pan African orogenic cycle in the Anti-Atlas Mountains,
676 Morocco. *Journal of African Earth Sciences*, *98*, 34-46.
677 Heuret, A., & Lallemand, S. (2005). Plate motions, slab dynamics and back-arc deformation. *Physics*
678 *of the Earth and Planetary Interiors*, *149*(1-2), 31-51.
679 Heuret, A., Funiciello, F., Faccenna, C., & Lallemand, S. (2007). Plate kinematics, slab shape and
680 back-arc stress: A comparison between laboratory models and current subduction zones. *Earth and*
681 *Planetary Science Letters*, *256*(3-4), 473-483.
682 Hodel, F., Macouin, M., Triantafyllou, A., Carlut, J., Berger, J., Rousse, S., N. Ennih & Trindade, R. I.
683 F. D. (2017). Unusual massive magnetite veins and highly altered Cr-spinels as relics of a Cl-rich acidic
684 hydrothermal event in Neoproterozoic serpentinites (Bou Azzer ophiolite, Anti-Atlas,
685 Morocco). *Precambrian Research*, *300*, 151-167.
686 Hodel, F., Macouin, M., Trindade, R. I. F., Triantafyllou, A., Ganne, J., Chavagnac, V., J. Berger, M.
687 Rospabé, C. Destrigneville, J. Carlut, N. Ennih & P. Agrinier, (2018). Fossil black smoker yields oxygen
688 isotopic composition of Neoproterozoic seawater. *Nature communications*, *9*(1), 1453.
689 Humphreys, E. (2009). Relation of flat subduction to magmatism and deformation in the western
690 United States. *Backbone of the Americas: Shallow subduction, plateau uplift, and ridge and terrane*
691 *collision*, *204*, 85.
692 Inglis, J. D., D'Lemos, R. S., Samson, S. D., & Admou, H. (2005). Geochronological constraints on
693 Late Precambrian intrusion, metamorphism, and tectonism in the Anti-Atlas Mountains. *The Journal of*
694 *geology*, *113*(4), 439-450.
695 Inglis, J. D., Hefferan, K., Samson, S. D., Admou, H., & Saquaque, A. (2017). Determining age of Pan
696 African metamorphism using Sm-Nd garnet-whole rock geochronology and phase equilibria modeling
697 in the Tasriwine ophiolite, Sirwa, Anti-Atlas Morocco. *Journal of African Earth Sciences*, *127*, 88-98.
698 Jagoutz, O. E., Burg, J. P., Hussain, S., Dawood, H., Pettke, T., Iizuka, T., & Maruyama, S. (2009).
699 Construction of the granitoid crust of an island arc part I: geochronological and geochemical constraints
700 from the plutonic Kohistan (NW Pakistan). *Contributions to Mineralogy and Petrology*, *158*(6), 739.

Jagoutz, O., & Behn, M. D. (2013). Foundering of lower island-arc crust as an explanation for the origin of the continental Moho. *Nature*, *504*(7478), 131.

Jagoutz, O., & Schmidt, M. W. (2013). The composition of the foundered complement to the continental crust and a re-evaluation of fluxes in arcs. *Earth and Planetary Science Letters*, *371*, 177-190.

Jicha, B. R., & Jagoutz, O. (2015). Magma production rates for intraoceanic arcs. *Elements*, *11*(2), 105-111.

Jochum, K. P., Nohl, U., Herwig, K., Lammel, E., Stoll, B., & Hofmann, A. W. (2005). GeoReM: a new geochemical database for reference materials and isotopic standards. Geostandards and Geoanalytical Research, 29(3), 333-338.

Jochum, K. P., Weis, U., Stoll, B., Kuzmin, D., Yang, Q., Raczek, I., & Günther, D. (2011). Determination of reference values for NIST SRM 610–617 glasses following ISO guidelines. Geostandards and Geoanalytical Research, 35(4), 397-429.

Jochum, K. P., Weis, U., Schwager, B., Stoll, B., Wilson, S. A., Haug, G. H., & Enzweiler, J. (2016). Reference values following ISO guidelines for frequently requested rock reference materials. *Geostandards and Geoanalytical Research*, *40*(3), 333-350.

Klein, E. M., & Langmuir, C. H. (2000). GERM [Geochemical Earth Reference Model] MORB data by ocean basin, depth, and MORB type: URL: *http://EarthRef. org/GERM/data/klein. MORB_ ocean.html*

Lallemand, S., Heuret, A., & Boutelier, D. (2005). On the relationships between slab dip, back-arc stress, upper plate absolute motion, and crustal nature in subduction zones. *Geochemistry, Geophysics, Geosystems*, *6*(9).

Lallemand, S., Heuret, A., Faccenna, C., & Funiciello, F. (2008). Subduction dynamics as revealed by trench migration. *Tectonics*, *27*(3).

Leat, P. T. and Larter, R. D. (2003). Intra-oceanic subduction systems: introduction. Geological Society, London, Special Publications, 219(1), 1-17.

Leat, P. T., Larter, R. D., & Millar, I. L. (2007). Silicic magmas of Protector Shoal, South Sandwich arc: indicators of generation of primitive continental crust in an island arc. *Geological Magazine*, *144*(1), 179-190.

Lee, C. T. A., & Anderson, D. L. (2015). Continental crust formation at arcs, the arclogite “delamination” cycle, and one origin for fertile melting anomalies in the mantle. *Science Bulletin*, *60*(13), 1141-1156.

Letsch, D., Houicha, M. E., von Quadt, A., & Winkler, W. (2017). A missing link in the peri-Gondwanan terrane collage: the Precambrian basement of the Moroccan Meseta and its lower Paleozoic cover. *Canadian Journal of Earth Sciences*, *55*(1), 33-51.

López, S., & Castro, A. (2001). Determination of the fluid–absent solidus and supersolidus phase relationships of MORB-derived amphibolites in the range 4–14 kbar. American Mineralogist, 86(11-12), 1396-1403.

Ludwig, K. R. (2003). Isoplot 3.00: A geochronological toolkit for Microsoft Excel. Berkeley Geochronology Center Special Publication, 4, 70.

Ma, Q., Zheng, J. P., Xu, Y. G., Griffin, W. L., & Zhang, R. S. (2015). Are continental “adakites” derived from thickened or foundered lower crust? Earth and Planetary Science Letters, 419, 125-133.

741 Mason, W. G., Moresi, L., Betts, P. G., & Miller, M. S. (2010). Three-dimensional numerical models of
742 the influence of a buoyant oceanic plateau on subduction zones. Tectonophysics, 483(1-2), 71-79.
743 Meffre, S., & Crawford, A. J. (2001). Collision tectonics in the New Hebrides arc (Vanuatu). *Island*
744 *Arc*, *10*(1), 33-50.
745 Miller, R. B., & Paterson, S. R. (2001). Influence of lithological heterogeneity, mechanical anisotropy,
746 and magmatism on the rheology of an arc, North Cascades, Washington. Tectonophysics, 342(3-4),
747 351-370.
748 Moghadam, H. S., Li, X. H., Santos, J. F., Stern, R. J., Griffin, W. L., Ghorbani, G., & Sarebani, N.
749 (2017). Neoproterozoic magmatic flare-up along the N. margin of Gondwana: The Taknar complex, NE
750 Iran. *Earth and Planetary Science Letters, 474, 83-96.*
751 Mrini, Z. (1993). Chronologie (Rb-Sr, U-Pb), traçage isotopique (Sr-Nd-Pb) des sources des roches
752 magmatiques éburnéennes, panafricaines et hercyniennes du Maroc. *Unpublished Thesis. University*
753 *of Marrakech, Maroc*.
754 Müntener, O., & Ulmer, P. (2018). Arc crust formation and differentiation constrained by experimental
755 petrology. *American Journal of Science*, *318*(1), 64-89
756 Nikolaeva, K., Gerya, T. V., & Connolly, J. A. (2008). Numerical modelling of crustal growth in
757 intraoceanic volcanic arcs. Physics of the Earth and Planetary Interiors, 171(1-4), 336-356.
758 Okada, S., & Ikeda, Y. (2012). Quantifying crustal extension and shortening in the back-arc region of
759 northeast Japan. *Journal of Geophysical Research: Solid Earth*, *117*(B1).
760 Palin, R. M., White, R. W., Green, E. C., Diener, J. F., Powell, R., & Holland, T. J. (2016). High-grade
761 metamorphism and partial melting of basic and intermediate rocks. Journal of Metamorphic Geology,
762 34(9), 871-892.
763 Paterson, S. R., & Ducea, M. N. (2015). Arc magmatic tempos: gathering the
764 evidence. *Elements*, *11*(2), 91-98.
765 Petterson, M. G., Babbs, T., Neal, C. R., Mahoney, J. J., Saunders, A. D., Duncan, R. A., & Natogga,
766 D. (1999). Geological–tectonic framework of Solomon Islands, SW Pacific: crustal accretion and growth
767 within an intra-oceanic setting. *Tectonophysics*, *301*(1-2), 35-60.
768 Profeta, L., Ducea, M. N., Chapman, J. B., Paterson, S. R., Gonzales, S. M. H., Kirsch, M., L. Petrescu
769 & DeCelles, P. G. (2015). Quantifying crustal thickness over time in magmatic arcs. *Scientific*
770 *Reports*, *5*, 17786.
771 Pubellier, M., Quebral, R., Aurelio, M., & Rangin, C. (1996). Docking and post-docking escape
772 tectonics in the southern Philippines. *Geological Society, London, Special Publications*, *106*(1), 511-
773 523.
774 Rioux, M., Mattinson, J., Hacker, B., Kelemen, P., Blusztajn, J., Hanghøj, K., & Gehrels, G. (2010).
775 Intermediate to felsic middle crust in the accreted Talkeetna arc, the Alaska Peninsula and Kodiak
776 Island, Alaska: An analogue for low-velocity middle crust in modern arcs. *Tectonics*, *29*(3).
777 Samson, S. D., Inglis, J. D., D'Lemos, R. S., Admou, H., Blichert-Toft, J., & Hefferan, K. (2004).
778 Geochronological, geochemical, and Nd–Hf isotopic constraints on the origin of Neoproterozoic
779 plagiogranites in the Tasriwine ophiolite, Anti-Atlas orogen, Morocco. *Precambrian Research*, *135*(1-2),
780 133-147.

781 Schellart, W. P., Freeman, J., Stegman, D. R., Moresi, L., & May, D. (2007). Evolution and diversity of
782 subduction zones controlled by slab width. *Nature*, *446*(7133), 308.
783 Sizova, E., Gerya, T., Brown, M., & Perchuk, L. L. (2010). Subduction styles in the Precambrian:
784 Insight from numerical experiments. Lithos, 116(3-4), 209-229.
785 Stern, R. J. (2010). The anatomy and ontogeny of modern intra-oceanic arc systems. *Geological*
786 *Society, London, Special Publications*, *338*(1), 7-34.
787 Sun, S. S., & McDonough, W. F. (1989). Chemical and isotopic systematics of oceanic basalts:
788 implications for mantle composition and processes. Geological Society, London, Special Publications,
789 42(1), 313-345.
790 Syracuse, E. M., & Abers, G. A. (2006). Global compilation of variations in slab depth beneath arc
791 volcanoes and implications. Geochemistry, Geophysics, Geosystems, 7(5).
792 Thomas, R. J., Chevallier, L. P., Gresse, P. G., Harmer, R. E., Eglington, B. M., Armstrong, R. A., C.H
793 de Beer, J.E. J Martini, G.S de Kock, P.H. Macey & Ingram, B. A. (2002). Precambrian evolution of the
794 Sirwa window, Anti-Atlas orogen, Morocco. *Precambrian Research*, *118*(1-2), 1-57.
795 Thomas, R. J., Fekkak, A., Ennih, N., Errami, E., Loughlin, S. C., Gresse, P. G., L.P. Chevallier &
796 Liégeois, J. P. (2004). A new lithostratigraphic framework for the Anti-Atlas Orogen, Morocco. *Journal*
797 *of African Earth Sciences*, *39*(3-5), 217-226.
798 Toummite, A., Liégeois, J. P., Gasquet, D., Bruguier, O., Beraaouz, E. H., & Ikenne, M. (2013). Field,
799 geochemistry and Sr-Nd isotopes of the Pan-African granitoids from the Tifnoute Valley (Sirwa, Anti-
800 Atlas, Morocco): a post-collisional event in a metacratonic setting. *Mineralogy and Petrology*, *107*(5),
801 739-763.
802 Triantafyllou, A., Berger, J., Baele, J. M., Bruguier, O., Diot, H., Ennih, N., C. Monnier, G. Plissart, S.
803 Vandycke, & Watlet, A. (2018). Intra-oceanic arc growth driven by magmatic and tectonic processes
804 recorded in the Neoproterozoic Bougmane arc complex (Anti-Atlas, Morocco). *Precambrian*
805 *Research*, *304*, 39-63.
806 Triantafyllou, A., Berger, J., Baele, J. M., Diot, H., Ennih, N., Plissart, G., C. Monnier, A. Watlet, O.
807 Bruguier, P. Spagna & Vandycke, S. (2016). The Tachakoucht–Iriri–Tourtit arc complex (Moroccan Anti-
808 Atlas): Neoproterozoic records of polyphased subduction-accretion dynamics during the Pan-African
809 orogeny. *Journal of Geodynamics*, *96*, 81-103.
810 Triantafyllou, A., Watlet, A., & Bastin, C. (2017). Geolokit: An interactive tool for visualising and
811 exploring geoscientific data in Google Earth. International journal of applied earth observation and
812 geoinformation, 62, 39-46.
813 Walsh, G. J., Benziane, F., Aleinikoff, J. N., Harrison, R. W., Yazidi, A., Burton, W. C., J. E. Quick &
814 Saadane, A. (2012). Neoproterozoic tectonic evolution of the jebel Saghro and Bou Azzer—El Graara
815 inliers, eastern and central Anti-Atlas, Morocco. *Precambrian Research*, *216*, 23-62.
816

Episodic magmatism during the growth of a Neoproterozoic oceanic arc (Anti-Atlas, Morocco)

Antoine Triantafyllou[1, 2], Julien Berger[3], Jean-Marc Baele[4], Nadine Mattielli[2], M. N. Ducea[1, 5], Sarane Sterckx[6], Scott Samson[7], Florent Hodel[3], Nasser Ennih[8]

[1] Department of Geosciences, University of Arizona, Tucson, Arizona 85721, USA.

[2] Department of Earth and Environmental Sciences – G-Time Laboratory, Université Libre de Bruxelles, 50 Avenue Franklin Roosevelt, 1050 Brussels, Belgium.

[3] Géosciences Environnement Toulouse (GET), Observatoire de Midi-Pyrénées, CNRS, IRD, Université de Paul Sabatier, UMR-CNRS 5563, 14, Avenue Edouard Belin, 31400 Toulouse, France.

[4] Department of Geology and Applied Geology, Université de Mons, 20, Place du Parc, B-7000, Belgium.

[5] Faculty of Geology and Geophysics, University of Bucharest, 010041, Bucharest, Romania.

[6] Goldspot Discoveries Inc., 69 Yonge Street Suite 1010, Toronto, Canada.

[7] Department of Earth Sciences, Syracuse University, Syracuse, NY 13244, USA.

[8] EGGPG, Département de Géologie, Faculté des Sciences, Université Chouaïb Doukkali, 24000 El Jadida, Morocco.

FIGURES and CAPTIONS

Figure 1

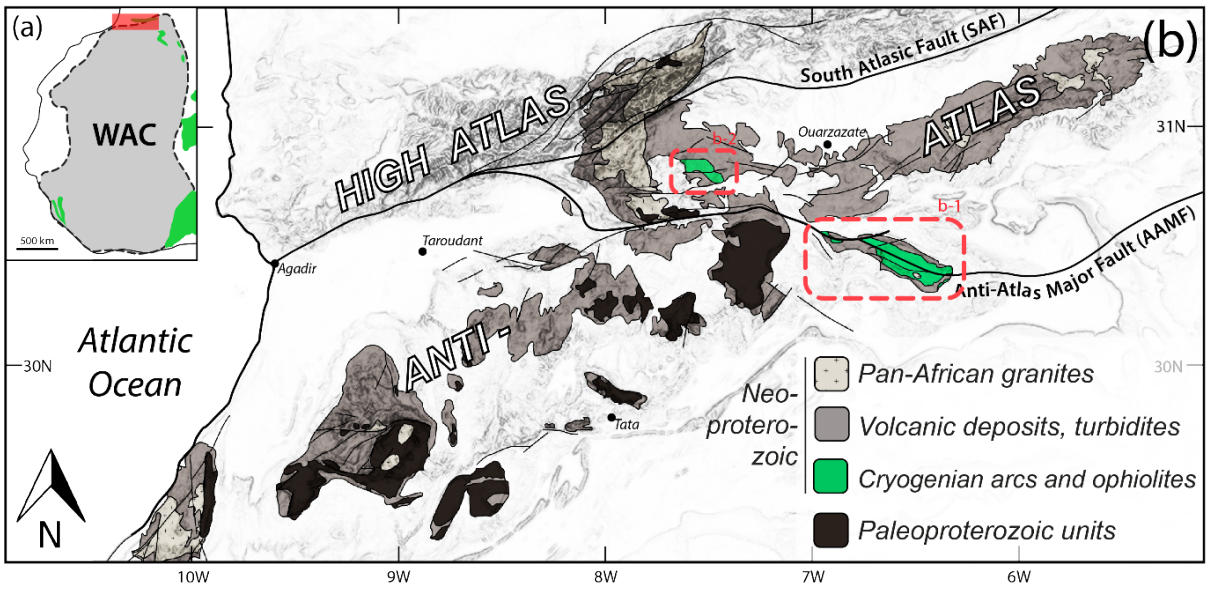

Figure 1 (a) Location of the studied area relatively to the West African Craton (WAC). Green is for Pan-African orogenic belt remnants. (b) Schematic map of the Precambrian inliers exposed in the Moroccan Anti-Atlas mountain belt (modified after Gasquet et al., 2008; basemap is Aster Gdem 2.0 topographic data) showing the Sirwa and the Bou Azzer - El Graara inliers to the W and the E, respectively.

Figure 2

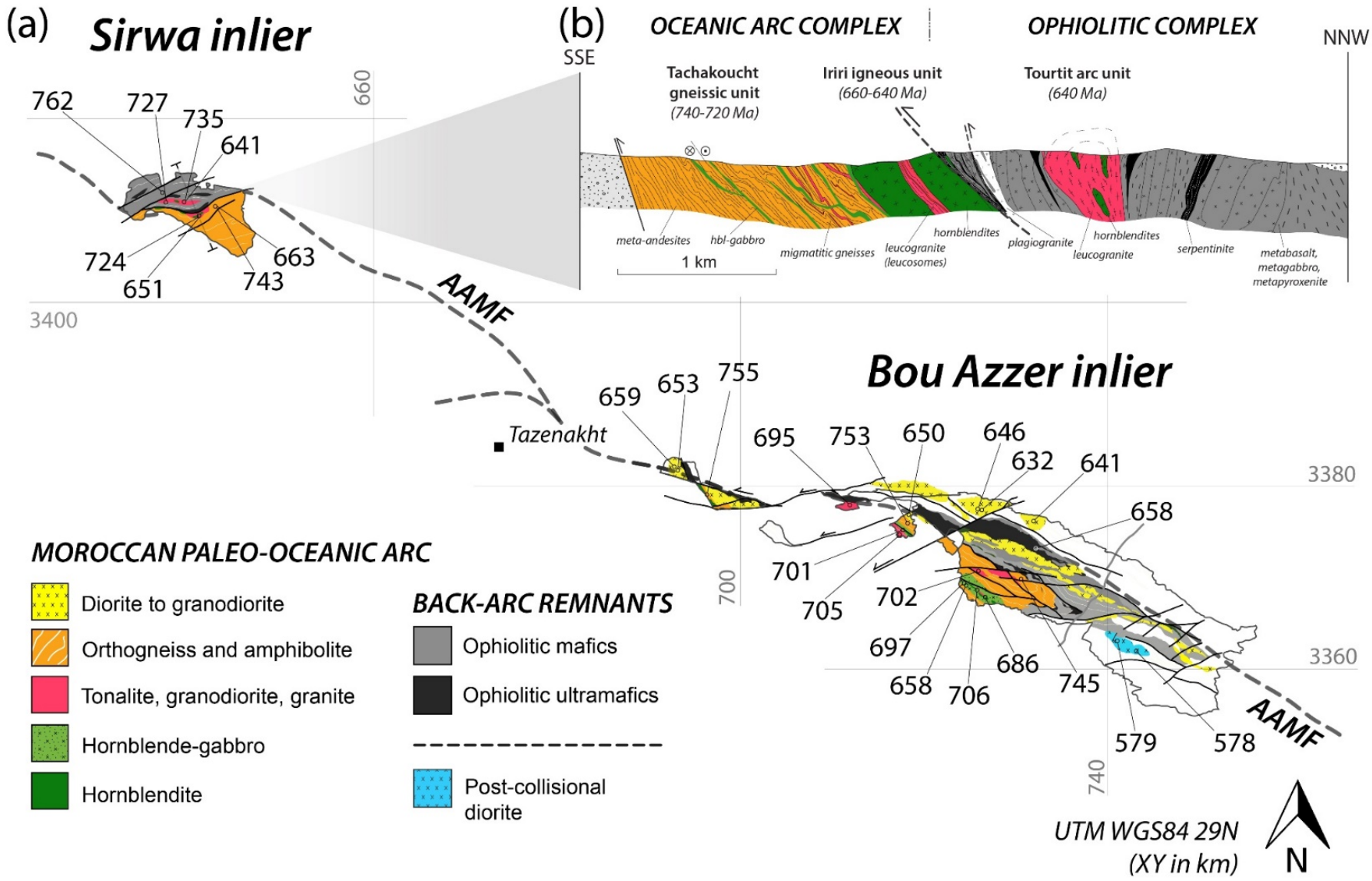
(a)
Sirwa inlier
762
727
735
641
724
651
743
663
660
3400
AAMF
(b)
SSE
NNW
OCEANIC ARC COMPLEX
OPHIOLITIC COMPLEX
Tachakoucht gneissic unit (740-720 Ma)
Iriri igneous unit (660-640 Ma)
Tourtit arc unit (640 Ma)
meta-andesites
hbl-gabbro
migmatitic gneisses
leucogranite (leucosomes)
hornblendites
plagiogranite
hornblendites
leucogranite
serpentinite
metabasalt, metagabbro, metapyroxenite
1 km
Bou Azzer inlier
Tazenakht
659
653
755
695
753
650
646
632
641
658
701
705
702
697
658
706
686
745
579
578
3380
3360
700
740
AAMF
MOROCCAN PALEO-OCEANIC ARC
Diorite to granodiorite
Orthogneiss and amphibolite
Tonalite, granodiorite, granite
Hornblende-gabbro
Hornblendite
BACK-ARC REMNANTS
Ophiolitic mafics
Ophiolitic ultramafics
Post-collisional diorite
UTM WGS84 29N
(XY in km)
N

Figure 2 (a) Simplified geological map of the igneous and meta-igneous units in the Sirwa (West) and the Bou Azzer inliers (East; modified after El Hadi et al., 2010; Triantafyllou et al., 2016). Geochronological data on plutonic and high-grade metamorphic/crystalline rock are gathered from literature (see appendix C1) and expressed in Ma. (b) Cross-section of the Sirwa arc-related units giving an overview of the relationships between arc and back-arc complexes. It shows the Iriri-Tachakoucht arc complex is thrusted by the Khzama back-arc ophiolitic sequence. This cross-section also highlights the emplacement of the Tourtit arc granitic unit into the ophiolitic sequence.

Figure 3

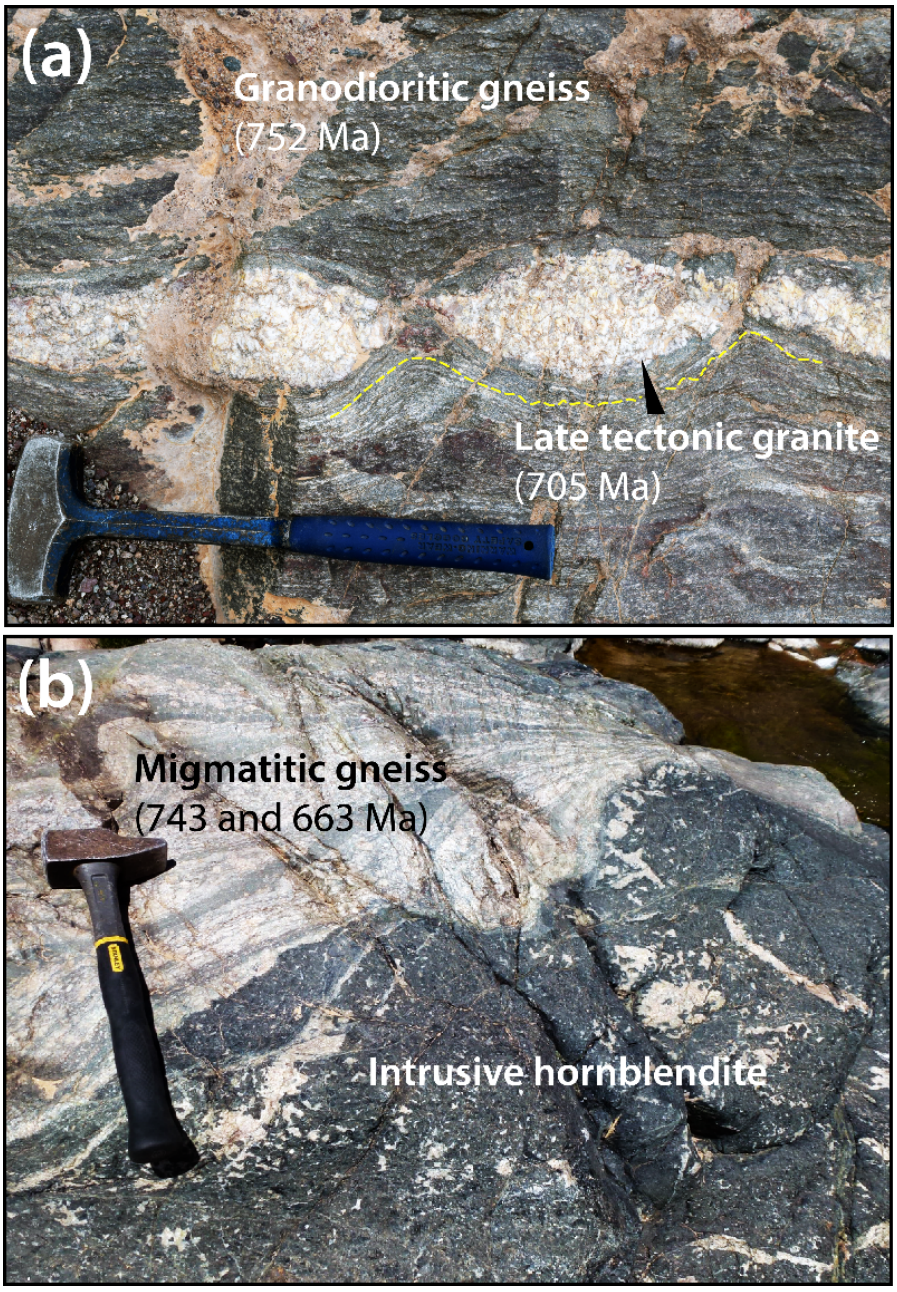

Figure 3 Field relations showing relative chronology between deformation and magmatic events. (a) Pseudo-boudinaged felsic dykes emplaced at 705 ± 3 Ma into 752 ± 2 Ma gneissic arc units (Tazigzaout complex, Bou Azzer inlier; D'Lemos et al., 2006). This field relation attests that the emplacement of felsic arc rock is concomitant to subsequent to the deformation event. (b) Hornblendite intruding meta-andesitic gneisses, marked by partial melting reactions of the host gneissic rocks and the development of felsic melts (Iriri-Tachakoucht arc complex, Sirwa inlier). Protolithic ages at 743 ± 14 Ma is from U-Pb method on zircon cores and high-

48 temperature metamorphic age at 663 ± 13 Ma on zircon rims in the host gneiss (Thomas et
49 al., 2002).
50

Figure 4

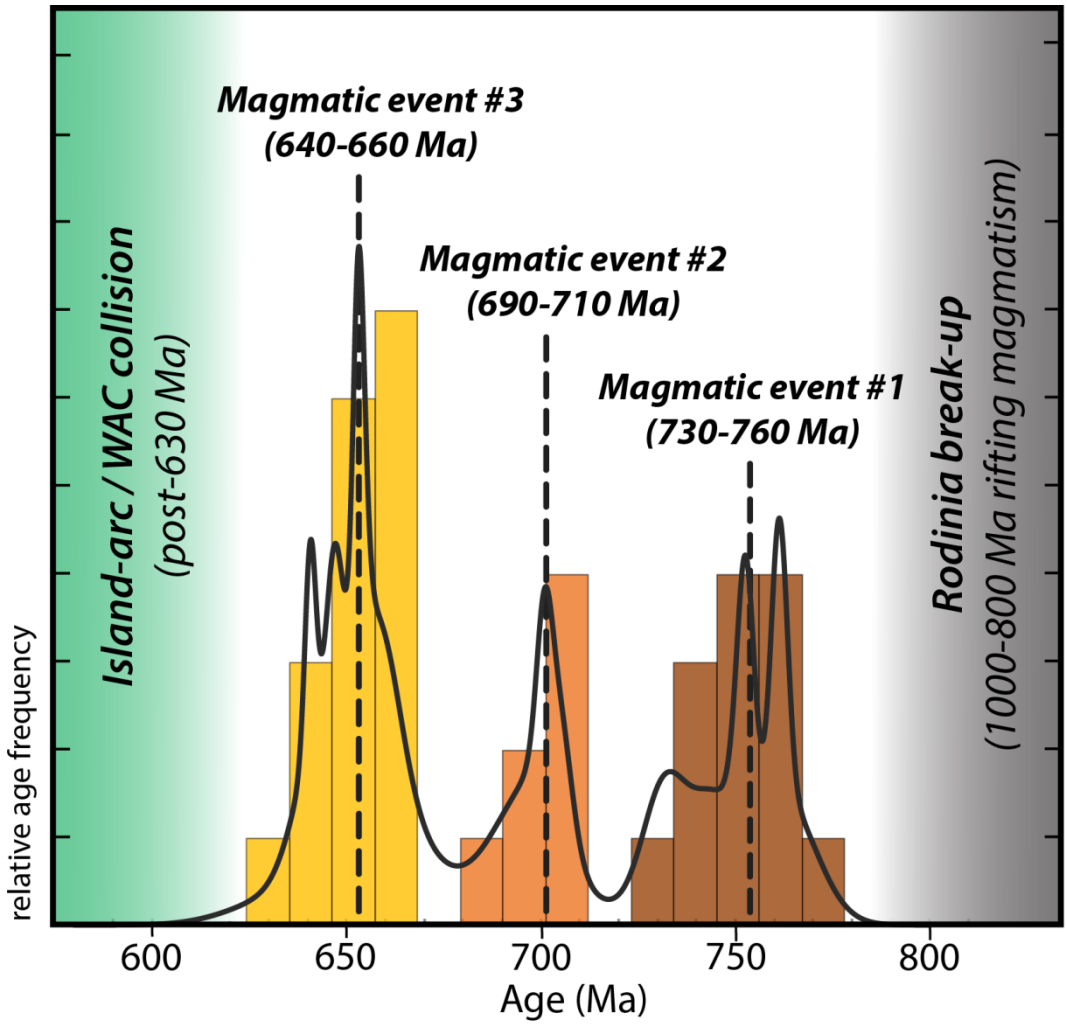

Figure 4 Frequency histogram of U-Pb ages (n = 37) displays the three magmatic events of oceanic arc-related activity that are discussed in the manuscript. Solid black line is a probability density function that weights each age determination according to its uncertainty and dashed black line median age value for each magmatic episode, *i.e.* Groups 1, 2 and 3. Probability density histogram has been calculated using Isoplot 3.0 (Ludwig, 2003).

Figure 5

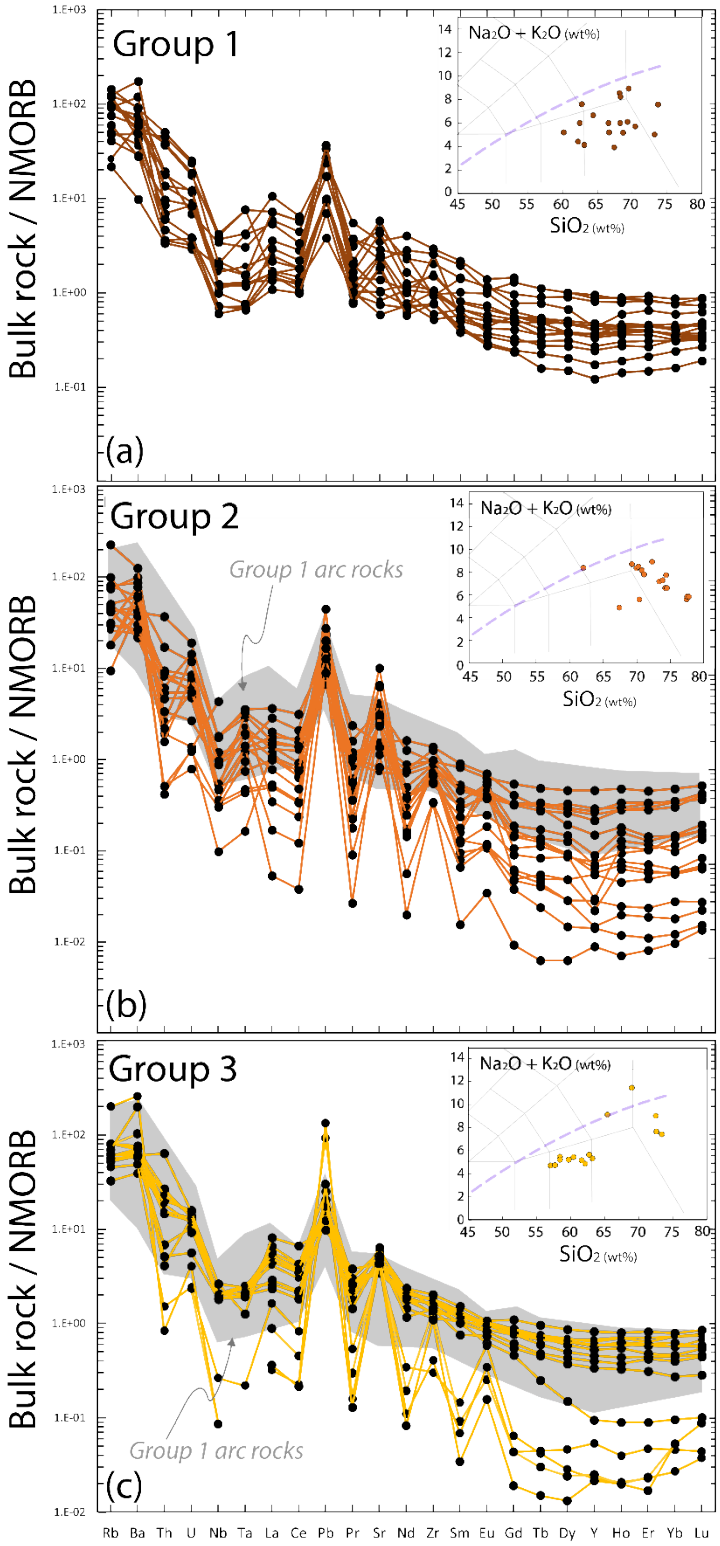

Figure 5 MORB-normalized spider diagram and TAS (Na_2O+K_2O *vs* SiO_2) diagrams for the intermediate to felsic arc lithologies of each age group of the Moroccan arc rocks classified per age group from the Moroccan arc complex. (a) Group1: 760-730 Ma, (b) Group2: 710-690 Ma and (c) Group3: 660-640 Ma. Trace element concentration is normalized to N-MORB values

from Sun and McDonough (1989). Blue dashed line is for alkaline-subalcaline transition after Le Bas et al. (1986).

Figure 6

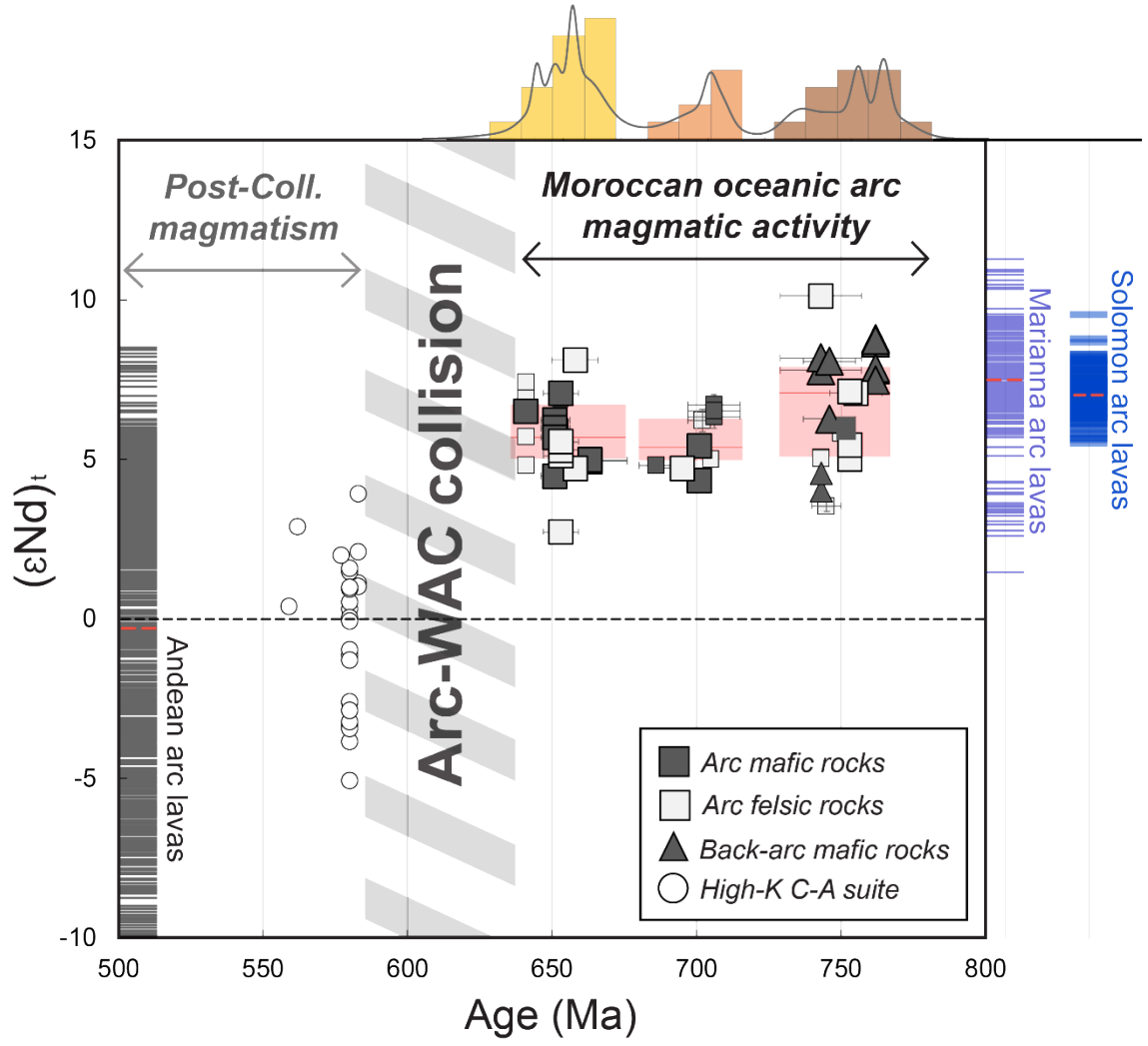

Figure 6 Nd isotopic data (□Nd_t) *vs* time (Ma) of Moroccan igneous arc rocks (modified after Triantafyllou et al., 2018). Large symbols show new isotopic data from this study. Small symbols are gathered from previous studies (D'Lemos et al., 2006; Beraaouz et al., 2004; Mrini, 1993). Isotopic data younger than 580 Ma are from post-collisional High-K Calc-Alkaline (HKCA) granitoids (Toummite et al., 2013; Mrini, 1993; Errami et al., 2009). Bar codes at both sides of the diagram display Nd isotopic data gathered from GEOROC database for Mariana intra-oceanic arc, Solomon transitional arc (right in blue) and Andean continental arc systems (left; error-weighted mean is marked by the red tick). Red boxes mark interquartile range (Q1-Q3) with the red line as median value.

Figure 7

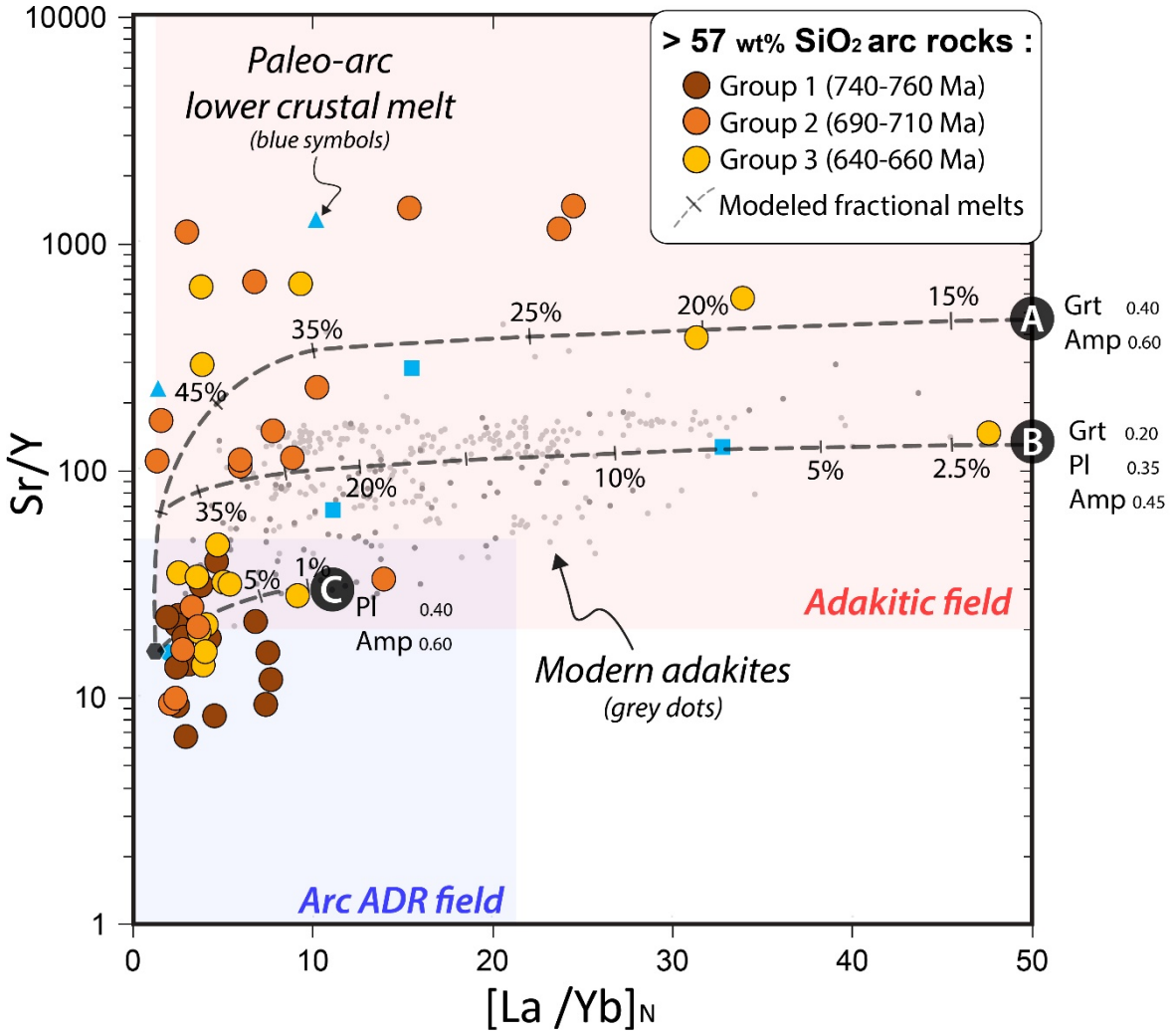

Figure 7 Evolution of depth sensitive (Sr/Y *vs* REE-normalized La/Yb) chemical composition of intermediate to felsic (meta-) igneous arc rocks (> 57 wt% SiO_2) for each age group of the Moroccan arc complex. Grey dashed lines show the composition of melt modelled by fractional melting of a hydrous mafic source. The model is based on typical concentrations in residual infra-arc rocks and averaged partition coefficients for dacitic and andesitic liquids referenced on GERM (Geochemical Earth Reference Model) online database available at http://earthref.org/KDD/ (Klein and Langmuir, 2000). Blue symbols are for felsic melt sampled at the root of Kohistan (triangle), Amalaoulaou (dot) and Fiordland (square) paleo-arc complexes.

Table C.1: Protolithic ages of Neoproterozoic (meta-) igneous arc rocks (Moroccan Anti-Atlas)

Lithology	Age (Ma)	error	Method	Locality	UTM_X	UTM_Y	Reference
Qtz diorite	632	9	U-Pb zircon	Bou Azzer - Bou Zben	724269	3378236	El Hadi et al, 2010
Qtz diorite	640.8	1	U-Pb zircon	Bou Azzer - Ousdrat	732149	3375147	Inglis et al, 2005
Orthogneiss leucosome	641	5	U-Pb zircon	Sirwa - Tourtit	639183	3410765	Triantafyllou et al., 2016
Qtz diorite	645	7	U-Pb zircon	Bou Azzer - Tafrawt	718038	3379664	Walsh et al., 2012
Qtz diorite	646	8	U-Pb zircon	Bou Azzer - Tamellalet	724289	3378248	Walsh et al., 2012
Garnet amphibolite	647	2	Sm-Nd garnet	Sirwa - Tourtit	639550	3410997.12	Inglis et al, 2016
Granodiorite	650	10	U-Pb zircon	Bou Azzer - Tazigzaout	718153	3376469	Walsh et al., 2012
Gneiss leucosome	651	5	U-Pb zircon	Sirwa - Tachakoucht	640658	3409398	Triantafyllou et al., 2016
Qtz diorite	653	1	U-Pb zircon	Bou Azzer - Bou Offroht	693058	3381216	Inglis et al., 2005
Diorite	653.8	2	U-Pb zircon	Bou Azzer - Ait Abdulla	742244	3372412	Inglis et al, 2005
Leucogranodiorite	658	8	U-Pb zircon	Bou Azzer	732752	3372919	Admou et al., 2013
Hornblende-gabbro	658	7	U-Pb rutile	Bou Azzer - Bougmane	724892	3368990	Triantafyllou et al., 2018
Granodiorite	659	5	U-Pb zircon	Bou Azzer - Bou Offroh	693066	3381085	El Hadi et al, 2010
Qtz diorite	659	5	U-Pb zircon	Bou Azzer - Bou Offroh	693066	3381085	El Hadi et al, 2010
Tonalitic migmatite	663	13	U-Pb zircon	Sirwa - Iriri-Tachakoucht	642196	3410179	Thomas et al, 2002
Diorite	667	11	U-Pb zircon	Bou Azzer	-	-	Mrini, 1993
Hornblendite	686	6	U-Pb rutile	Bou Azzer - Bougmane	726041	3368260	Triantafyllou et al., 2018
Leucogranite	695	7	U-Pb zircon	Bou Azzer - Oumlill	711742	3377808	Admou et al., 2013
Metagabbro	697	8	U-Pb zircon	Bou Azzer - Bougmane	724893	3368999	El Hadi et al, 2010
Leucogranite	701	2	U-Pb zircon	Bou Azzer - Tazigzaout	717674	3374755	D'Lemos et al., 2006
Tonalite	702	5	U-Pb zircon	Bou Azzer - Bougmane	725744	3369976	Admou et al., 2013
Leucogranite	705	3	U-Pb zircon	Bou Azzer - Tazigzaout	717112	3374506	D'Lemos et al., 2006
Hornblende-gabbro	706	9	U-Pb zircon	Bou Azzer - Bougmane	724892	3368990	Triantafyllou et al., 2018
Gneiss protolith	727	5	U-Pb zircon	Sirwa - Tachakoucht	637738	3410731	Triantafyllou et al., 2016
Gneiss protolith	724	7	U-Pb zircon	Sirwa - Tachakoucht	640658	3409398	Triantafyllou et al., 2016
Orthogneiss protolith	735	7	U-Pb zircon	Sirwa - Tourtit	639183	3410765	Triantafyllou et al., 2016
Orthogneiss protolith	741	9	U-Pb zircon	Bou Azzer - Oumlill	711797/	3377805	El Hadi et al, 2010
Tonalitic migmatite	743	14	U-Pb zircon	Sirwa - Tachakoucht	642196	3410179	Thomas et al, 2002
Orthogneiss protolith	745	5	U-Pb zircon	Bou Azzer - Bougmane	730335	3368504	Admou et al., 2013
Orthogneiss protolith	751	10	U-Pb zircon	Bou Azzer - Oumlill	730335	3368504	Admou et al., 2013

Table C.1: Protolithic ages of Neoproterozoic (meta-) igneous arc rocks (Moroccan Anti-Atlas)

Lithology	Age (Ma)	error	Method	Locality	UTM_X	UTM_Y	Reference
Metagabbro	752.2	2	U-Pb zircon	Bou Azzer - Tazigzaout	717675	3374766	D'Lemos et al., 2006
Granite gneiss	753	2	U-Pb zircon	Bou Azzer - Tazigzaout	718094	3375619	D'Lemos et al., 2006
Orthogneiss protolith	755	9	U-Pb zircon	Bou Azzer - Bougmane-Takrou	696363	3379078	Admou et al., 2013
Plagiogranite	761	2	U-Pb zircon	Sirwa - Khzama	636198	3411112	Samson et al, 2004
Volcanic arc rocks	761	7	U-Pb zircon	Bou Azzer	742066	3371557	Admou et al., 2013
Plagiogranite	762	2	U-Pb zircon	Sirwa - Khzama	636198	3411112	Samson et al, 2004
Volcanic arc rocks	767	7	U-Pb zircon	Bou Azzer	756142	3364083	Admou et al., 2013

Table C.2: Nd Isotopic data on Neoproterozoic arc rocks (Moroccan Anti-Atlas)

Lithology	Sample	Sm (ppm)	Nd (ppm)	$^{147}Sm/^{144}Nd$	$^{143}Nd/^{144}Nd$	2σ	Age (Ma)	εNd(t)
Metagabbro	TAW21b	1.74	4.10	0.256641	0.513380	0.000010	762	8.7
Metagabbro	TAW21b bis	1.74	4.10	0.256641	0.513387	0.000010	762	8.8
Microgabbro	TAW 29	4.50	17.30	0.157300	0.512845	0.000010	743	7.8
Metabasalt	TAW30	2.80	7.10	0.238485	0.513260	0.000008	743	8.2
Metabasalt	TAW46	7.30	37.00	0.119311	0.512651	0.000012	762	7.8
Metabasalt	TAW46b	7.30	37.00	0.119311	0.512652	0.000008	762	7.8
Metabasalt	TAW49	2.70	7.80	0.209329	0.513147	0.000009	762	8.7
Metagabbro	TAW82	0.80	2.40	0.201576	0.513065	0.000010	762	7.9
Microgabbro	TA11	1.36	3.08	0.267197	0.513373	0.000015	762	7.5
Metagabbro	L42	2.61	11.37	0.138878	0.512768	0.000010	746	8.1
Metagabbro	L62	5.23	18.59	0.170131	0.512828	0.000007	746	6.3
Hornblende-gabbro	TAW59	8.60	39.00	0.133351	0.512615	0.000010	663	4.9
Hornblende-gabbro	TAW59b	8.60	39.00	0.133351	0.512617	0.000008	663	5.0
Hornblende-gabbro	TAW62b	3.40	12.40	0.165813	0.512825	0.000010	651	6.2
Hornblende-gabbro	TA1	2.51	6.80	0.223216	0.513057	0.000011	651	6.0
Metabasalt	TA4	2.91	13.64	0.128960	0.512640	0.000014	651	5.7
Metabasalt	LH5B	1.00	2.49	0.243835	0.513068	0.000015	651	4.5
Hornblende-gabbro	TA44	2.78	9.49	0.177121	0.512888	0.000012	641	6.5
Hornblende-gabbro	BB3c	3.29	13.71	0.145117	0.512779	0.000009	653	7.1
Hornblende-gabbro	BB16	3.15	10.03	0.190015	0.512829	0.000009	701	4.3
Hornblende-gabbro	BB16b	3.35	11.07	0.183003	0.512852	0.000006	701	5.4
Orthogneiss	TAW8b	0.42	2.00	0.126993	0.512816	0.000011	743	10.1
Diorite intrusive	AB43	2.66	13.89	0.115850	0.512704	0.000009	658	8.1
Diorite intrusive	AB45	3.59	15.25	0.142208	0.512644	0.000007	658	4.7
Hornblende-diorite	BB2A	2.76	10.52	0.158655	0.512614	0.000008	653	2.7
Diorite	BB3	3.29	12.76	0.155922	0.512725	0.000007	653	5.1
Diorite	BB3b	3.29	12.76	0.155922	0.512734	0.000009	653	5.3
Qtz Diorite	BB3c	3.29	12.76	0.155922	0.512747	0.000007	653	5.5
Dioritic gneiss	BB6	1.00	4.25	0.142289	0.512731	0.000015	755	7.1
Metagranite	OM8	0.91	3.61	0.152439	0.512678	0.000013	695	4.7

Table C.2: Nd Isotopic data on Neoproterozoic arc rocks (Moroccan Anti-Atlas)

Lithology	Sample	Sm (ppm)	Nd (ppm)	$^{147}Sm/^{144}Nd$	$^{143}Nd/^{144}Nd$	2σ	Age (Ma)	eNd(t)
Granodioritic gneiss	TT2	0.51	1.76	0.175234	0.512788	0.000007	753	5.0
Granodioritic gneiss	TT7A	3.83	15.91	0.145576	0.512750	0.000009	753	7.1
Augen granitic gneiss	TT12	1.09	5.26	0.125315	0.512564	0.000008	753	5.4